cGAS-STING drives the IL-6-dependent survival of chromosomally instable cancers

Hong, Christy; Schubert, Michael; Tijhuis, Andréa E; Requesens, Marta; Roorda, Maurits; van den Brink, Anouk; Ruiz, Lorena Andrade; Bakker, Petra L; van der Sluis, Tineke; Pieters, Wietske

Published in:
Nature

DOI:
10.1038/s41586-022-04847-2

Publication date:
2022

Article

cGAS–STING drives the IL-6-dependent survival of chromosomally instable cancers

https://doi.org/10.1038/s41586-022-04847-2

Received: 1 September 2021

Accepted: 10 May 2022

Published online: 15 June 2022

Check for updates

Christy Hong[1], Michael Schubert[1,6,7], Andréa E. Tijhuis[1,7], Marta Requesens[1,2,7], Maurits Roorda[3], Anouk van den Brink[1], Lorena Andrade Ruiz[1], Petra L. Bakker[1], Tineke van der Sluis[4], Wietske Pieters[5], Mengting Chen[3], René Wardenaar[1], Bert van der Vegt[4], Diana C. J. Spierings[1], Marco de Bruyn[2]✉, Marcel A. T. M. van Vugt[3]✉ & Floris Foijer[1]✉

Chromosomal instability (CIN) drives cancer cell evolution, metastasis and therapy resistance, and is associated with poor prognosis[1]. CIN leads to micronuclei that release DNA into the cytoplasm after rupture, which triggers activation of inflammatory signalling mediated by cGAS and STING[2,3]. These two proteins are considered to be tumour suppressors as they promote apoptosis and immunosurveillance. However, cGAS and STING are rarely inactivated in cancer[4], and, although they have been implicated in metastasis[5], it is not known why loss-of-function mutations do not arise in primary tumours[4]. Here we show that inactivation of cGAS–STING signalling selectively impairs the survival of triple-negative breast cancer cells that display CIN. CIN triggers IL-6–STAT3-mediated signalling, which depends on the cGAS–STING pathway and the non-canonical NF-κB pathway. Blockade of IL-6 signalling by tocilizumab, a clinically used drug that targets the IL-6 receptor (IL-6R), selectively impairs the growth of cultured triple-negative breast cancer cells that exhibit CIN. Moreover, outgrowth of chromosomally instable tumours is significantly delayed compared with tumours that do not display CIN. Notably, this targetable vulnerability is conserved across cancer types that express high levels of IL-6 and/or IL-6R in vitro and in vivo. Together, our work demonstrates pro-tumorigenic traits of cGAS–STING signalling and explains why the cGAS–STING pathway is rarely inactivated in primary tumours. Repurposing tocilizumab could be a strategy to treat cancers with CIN that overexpress IL-6R.

CIN is poorly tolerated by untransformed cells, yet occurs frequently in cancer, which suggests that cancer cells have developed adaptations to overcome aneuploidy-imposed stresses that include proteotoxic stress, metabolic stress and an inflammatory response[6]. Modulating these stress pathways may therefore provide an Achilles' heel of cancers with a CIN phenotype. Indeed, exacerbation of proteotoxic stress or metabolic stress can be more toxic to aneuploid cells than to euploid cells in vitro[7]. However, effective approaches to exploit CIN-induced inflammation have not yet been identified and none has been validated in vivo.

Cells with CIN depend on cGAS and STING

To explore the effect of modulation of the inflammatory response in cells displaying CIN, we investigated the cGAS–STING pathway in triple-negative breast cancer (TNBC) cells. To induce micronuclei formation and to activate cGAS–STING signalling in human BT549 TNBC cells, cells were treated with the MPS1 inhibitor reversine[8] or the WEE1 inhibitor AZD1775 (ref. [9]). Both treatments significantly increased the frequency of mitotic abnormalities (Fig. 1a,b and Extended Data Fig. 1a) and micronuclei (Extended Data Fig. 1b,c). MPS1 inhibition mostly produced micronuclei that included centromeres, which reflects whole chromosome missegregation events. By contrast, WEE1 inhibition mostly produced micronuclei without centromeres (Extended Data Fig. 1d,e), which indicates that structural chromosomal abnormalities resulted from WEE1-inhibition-induced replication stress[10] (Extended Data Fig. 1f). Approximately half of the micronuclei were positive for cGAS (Extended Data Fig. 1b,c), which coincided with strong activation of cGAS signalling. This was quantified by the steep increase in both intracellular and extracellular cGAMP (Extended Data Fig. 1g), which is a direct readout of cGAS activation[11]. In line with this notion, MPS1 inhibition also promoted perinuclear localization of STING (Extended Data Fig. 1h,i), a downstream player of cGAS signalling that is activated by cGAMP[12,13]. Moreover, MPS1 inhibition led to increased phosphorylation

[1]European Research Institute for the Biology of Ageing, University of Groningen, University Medical Center Groningen, Groningen, The Netherlands. [2]Department of Obstetrics and Gynaecology, University of Groningen, University Medical Center Groningen, Groningen, The Netherlands. [3]Department of Medical Oncology, University of Groningen, University Medical Center Groningen, Groningen, The Netherlands. [4]Department of Pathology and Medical Biology, University of Groningen, University Medical Center Groningen, Groningen, The Netherlands. [5]Division of Tumor Biology and Immunology, Netherlands Cancer Institute, Amsterdam, The Netherlands. [6]Present address: Division of Cell Biology and Cancer Genomics Center, Netherlands Cancer Institute, Amsterdam, The Netherlands. [7]These authors contributed equally: Michael Schubert, Andréa E. Tijhuis, Marta Requesens. ✉e-mail: m.de.bruyn@umcg.nl; m.vugt@umcg.nl; f.foijer@umcg.nl

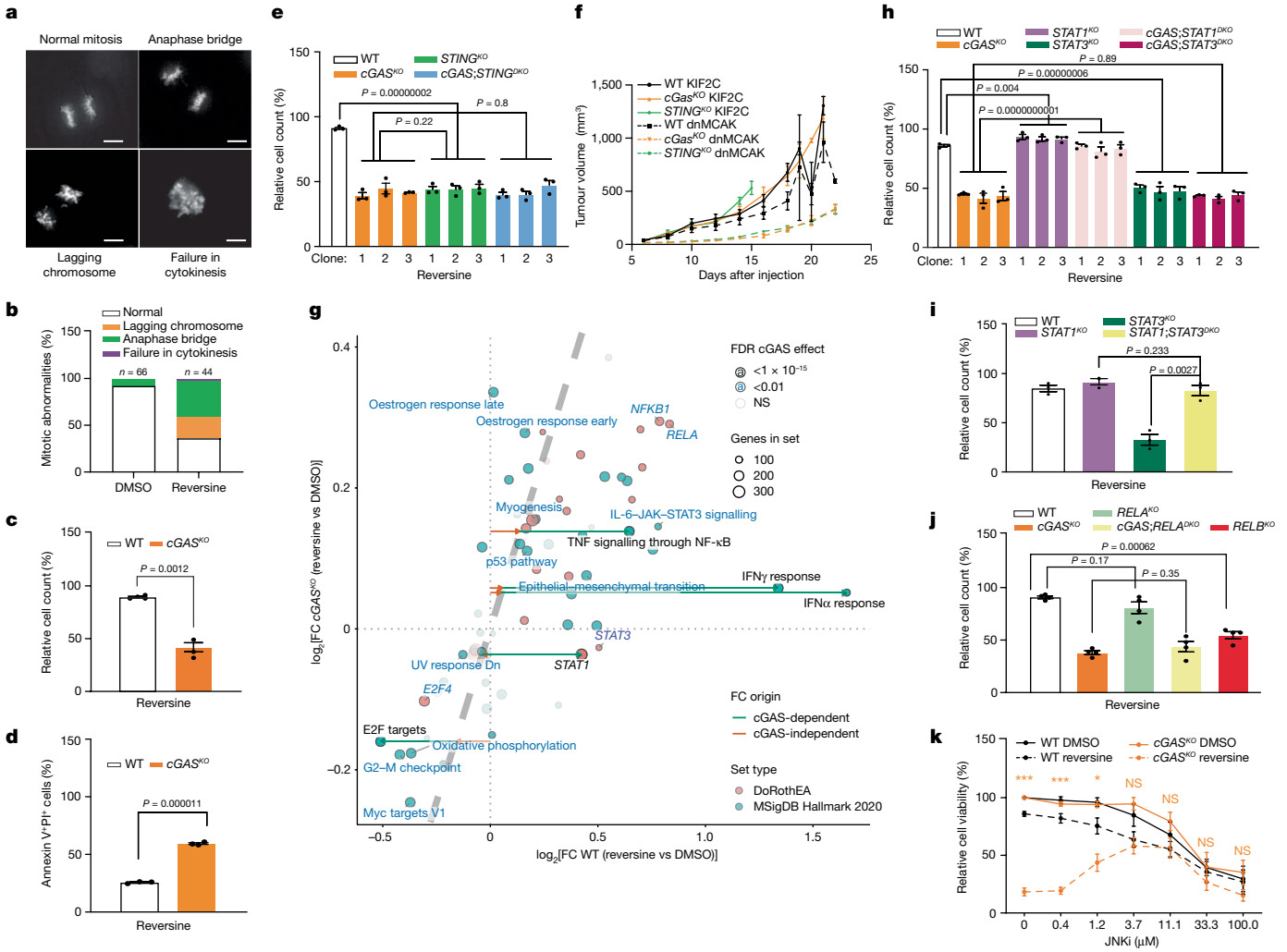

Fig. 1 | Loss of cGAS–STING-mediated signalling impairs the proliferation of TNBC cells that display CIN. a, Representative live-cell microscopy images of BT549 cells expressing histone H2B–mCherry. Scale bar, 10 μm. **b**, Quantification of mitotic abnormalities in BT549 cells expressing histone H2B–mCherry treated with dimethyl sulfoxide (DMSO) or 250 nM reversine. **c**, DMSO-normalized cell count of wild-type (WT) or *cGAS*^{KO} BT549 cells treated with 250 nM reversine. **d**, Fraction of apoptotic cells determined by Annexin V^{+} staining of WT and c*GAS*^{KO} BT549 cells treated with 250 nM reversine. PI, propidium iodide. **e**, DMSO-normalized cell count of WT, c*GAS*^{KO}, *STING*^{KO} and *cGAS;STING*^{DKO} cells treated with 250 nM reversine. **f**, Average tumour size over time observed for KIF2C (CIN^{low}) or dnMCAK (CIN^{high}) WT, *cGas*^{KO} or *STING*^{KO} 4T1 cells allografted into Balb/c mice. **g**, Characterization of the gene expression response of reversine-treated WT (*x* axis) or *cGAS*^{KO} (*y* axis) BT549 cells. Gene sets along the dashed grey line are changed equally in both genotypes, whereas more extreme values on the *x* axis indicate that they are primarily driven by cGAS. **h**–**j**, DMSO-normalized cell counts of the following BT549 cells treated with 250 nM reversine: WT, *cGAS*^{KO}, *STAT1*^{KO}, *cGAS;STAT1*^{DKO}, *STAT3*^{KO} and *cGAS;STAT3*^{DKO} (**h**); WT, *STAT1*^{KO}, *STAT3*^{KO}, *STAT1;STAT3*^{DKO} (**i**); and WT, *cGAS*^{KO}, *RELA*^{KO}, *cGAS;RELA*^{DKO} and *RELB*^{KO} (**j**). **k**, Cell viability of DMSO-treated or reversine-treated (250 nM) WT and *cGAS*^{KO} BT549 cells across a range of JNK inhibitor (JNKi) concentrations. Error bars in **c**–**f** and **h**–**k** represent the s.e.m., $n = 4$ biological replicates (**c**,**j**), $n = 3$ biological replicates (**d**–**e**,**h**–**i**,**k**), $n = 8$ biological replicates (**f**). Significance was tested with two-sided *t*-test (**c**–**e**,**h**–**k**). $^{*}P < 0.05$, $^{**}P < 0.01$, $^{***}P < 0.005$ (**k**). Exact *P* values are specified in the source data. Cells were treated for 72 h.

of IRF3, STAT1 and STAT3, all established readouts of activated cGAS–STING signalling[14–16] (Extended Data Fig. 1j). We conclude that cGAS–STING signalling is efficiently activated by the numerical and structural CIN induced by MPS1 and WEE1 inhibition, respectively.

To assess the importance of cGAS activation in cells with CIN, we used CRISPR–Cas9 to knock out *cGAS* in BT549 cells (*cGAS*^{KO}) (Extended Data Fig. 2a). As expected, when treated with MPS1 or WEE1 inhibitors, *cGAS*^{KO} cells did not produce cGAMP (Extended Data Fig. 2b), showed little to no increase in perinuclear STING (Extended Data Fig. 2c,d) and did not show induction of IRF3, STAT1 or STAT3 phosphorylation (Extended Data Fig. 2e). However, *cGAS*^{KO} cells were more sensitive to MPS1 and WEE1 inhibition than wild-type cells (*cGAS*^{WT}), as evidenced by their decreased cell viability and increased Annexin V positivity (Fig. 1c,d and Extended Data Fig. 2f,g). Similarly, blockade of cGAS activity using the cGAS inhibitor RU.521 (ref. [17]) significantly decreased the viability of BT549 cells treated with MPS1 and WEE1 inhibitors (Extended Data Fig. 2h,i). Of note, *cGAS* inactivation itself did not alter CIN phenotypes (Extended Data Fig. 2j). CRISPR-mediated inactivation of *STING* (Extended Data Fig. 2k) produced the same phenotype. That is, a failure to activate IRF3, STAT1 and STAT3 following MPS1 inhibition (Extended Data Fig. 2e), and increased sensitivity to MPS1 and WEE1 inhibition, which was not exacerbated in cells in which both *cGAS* and *STING* are knocked out (*cGAS;STING*^{DKO}) (Fig. 1e and Extended Data Fig. 2l). These findings indicate that cGAS exclusively signals through STING in this context.

In parallel, we tested the effect of CRISPR–Cas9-mediated *cGas* inactivation in 4T1 mouse TNBC cells (Extended Data Fig. 3a). *cGas*^{KO} 4T1 cells displayed reduced perinuclear STING localization when treated with the

MPS1 inhibitor (Extended Data Fig. 3b,c). Furthermore, treatment with either the MPS1 or WEE1 inhibitor induced CIN as expected (Extended Data Fig. 3d), and decreased viability and increased apoptosis of *cGas*^{KO} 4T1 cells compared with wild-type 4T1 cells and untreated wild-type or *cGas*^{KO} 4T1 cells (Extended Data Fig. 3e–h). Thus, cGAS–STING signalling promotes survival in TNBC cells with drug-induced, that is, acute CIN.

Next, we studied the cGAS–STING response in TNBC cells in which we induced chronic CIN. For this purpose, we engineered mouse TNBC 4T1 cell lines (wild-type, *cGas*^{KO} and *STING*^{KO}; Extended Data Fig. 3a) that overexpressed the kinesin-13 protein MCAK (also known as KIF2C) or a dominant-negative mutant form of MCAK (dnMCAK). This is an established method to produce CIN^{low} or CIN^{high} phenotypes, respectively[18]. CIN rates were confirmed by time-lapse microscopy (Extended Data Fig. 3i). Similar to MPS1 or WEE1 inhibitor treatment, dnMCAK induced phosphorylation of IRF3, STAT1 and STAT3 in 4T1 wild-type cells, which was mitigated in *cGas*^{KO} and *STING*^{KO} 4T1 cells (Extended Data Fig. 3j). Although dnMCAK expression reduced proliferation in all three genotypes, it affected the proliferation of *cGas*^{KO} and *STING*^{KO} cells more than wild-type 4T1 cells, which is in agreement with our findings with MPS1 and WEE1 inhibitors (Extended Data Fig. 3k).

We also tested whether impaired cGAS–STING signalling affected tumour growth in vivo. For this purpose, we allografted 4T1 wild-type, *cGas*^{KO} and *STING*^{KO} cells into Balb/c mice (4T1 cells are Balb/c-derived[19]). This in vivo experiment showed that dnMCAK delayed growth most significantly for *cGas*^{KO} and *STING*^{KO} cells, leading to smaller tumours that arose later (Fig. 1f and Extended Data Fig. 3l,m). Therefore, the dependence on functional cGAS signalling to tolerate CIN is not specific to BT549 or even human TNBC cell lines and occurs in vivo. We conclude that loss of cGAS–STING signalling sensitizes BT549 and 4T1 TNBC cells to both acute CIN induced by MPS1 and WEE1 inhibition and chronic CIN induced by dnMCAK. This result suggests that cGAS–STING signalling is crucial for coping with CIN in vitro and in vivo.

Cells with CIN rely on STAT3 and NF-κB

To assess the extent to which inflammatory signalling is affected by cGAS inactivation, we compared transcriptomes of treated and untreated wild-type and *cGAS*^{KO} BT549 cells in which MPS1 was inhibited to induce CIN. MPS1 inhibition triggered a strong induction of interferon (IFN)–STAT1–STAT3 signalling and TNF–NF-κB signalling in wild-type cells, which was reduced in *cGAS*^{KO} cells. This reduction was most significant for IFN–STAT1–STAT3 signalling and to a lesser extent for TNF–NF-κB signalling (Fig. 1g and Extended Data Fig. 4). Furthermore, induction of expression of the cGAS–STING-regulated cytokines CCL5 and CXCL10 (ref. [20]) was significantly reduced in *cGAS*^{KO}, *STING*^{KO} and *cGAS;STING*^{DKO} BT549 cells following MPS1 inhibition (Extended Data Fig. 5a). Similarly, *cGas*^{KO} and *STING*^{KO} 4T1 cells failed to induce CCL5 and CXCL10 expression in response to expression of dnMCAK (Extended Data Fig. 5b), which confirms that inactivation of cGAS or STING reduces inflammatory signalling in human and mouse cells, as expected[20]. Because of these observations, and as *cGAS*^{KO} and *STING*^{KO} cells failed to induce phosphorylation of STAT1 and STAT3 following CIN (Extended Data Fig. 2e), we inactivated *STAT1* (Extended Data Fig. 5c) and *STAT3* (Extended Data Fig. 5d) using CRISPR–Cas9. Inactivation of either *STAT1* or *STAT3* mitigated acute CIN-induced CCL5 and CXCL10 expression (Extended Data Fig. 5a), whereas only STAT3 inactivation sensitized *cGAS*^{WT} cells to MPS1 inhibitor treatment similar to *cGAS* inactivation (Fig. 1h and Extended Data Fig. 5e). Conversely, inactivation of *STAT1* in *cGAS*^{KO} cells largely rescued the sensitivity to either inhibitor (Fig. 1h and Extended Data Fig. 5e). This was also true when we induced chronic CIN through dnMCAK expression in these cell lines (Extended Data Fig. 5f). Enhancement of mitotic fidelity in dnMCAK-expressing genotypes using the small-molecule compound UMK57 (ref. [21]) increased the viability of *cGAS*^{KO} and *STAT3*^{KO} cells (Extended Data Fig. 5g). This provides further proof that loss of viability in these genotypes resulted from increased CIN rates imposed by dnMCAK. Taken together, these results indicate that acute and chronic CIN reduce the viability of *STAT3*^{KO}, but not *STAT1*^{KO}, cells and furthermore suggest that STAT1 activation promotes cell death following inhibitor treatment.

To functionally test whether STAT1 activation promotes cell death, we expressed wild-type, constitutively active (STAT1^{Y701E}) or non-phosphorylatable (STAT1^{Y701A}) versions of STAT1 in a doxycycline-inducible manner in wild-type, *cGAS*^{KO} and *STAT3*^{KO} BT549 cells (Extended Data Fig. 5h). Overexpression of STAT1^{Y701E}, and to a lesser extent wild-type STAT1, but not STAT1^{Y701A}, reduced the viability of wild-type, *cGAS*^{KO} and *STAT3*^{KO} cells and further increased the sensitivity to MPS1 inhibition in a dose-dependent manner (Extended Data Fig. 5i). This indicates that STAT1 phosphorylation promotes cell death induced by MPS1 and WEE1 inhibition in all three genotypes. Conversely, concomitant *STAT1* inactivation in *STAT3*^{KO} cells completely abrogated MPS1 and WEE1 inhibitor-mediated cell death (Fig. 1i and Extended Data Fig. 5c). Together, these findings are in good agreement with known roles for STAT1 in promoting cell death and STAT3 in promoting cell survival in cancer cells[22] and following viral infection[23,24].

To determine the relative importance of canonical (RELA-mediated) and non-canonical (RELB-mediated) NF-κB signalling, we generated *RELA*^{KO} and *RELB*^{KO} BT549 cells (Extended Data Fig. 6a,b) and tested the impact of drug-induced CIN on these cell lines. *RELA* inactivation did not change the response to MPS1 or WEE1 inhibition, neither did it alter the phenotype of *cGAS*^{KO} cells (Fig. 1j and Extended Data Fig. 6c). By contrast, loss of RELB sensitized cells to both MPS1 and WEE1 inhibition, as observed in *cGAS*^{KO} cells (Fig. 1j and Extended Data Fig. 6c). A similar increased sensitivity to MPS1 and WEE1 inhibition was seen following inactivation of *NIK* (Extended Data Fig. 6d–f), a known activator of non-canonical NF-κB signalling[25], but not in cells in which we inactivated *TRAF2* (Extended Data Fig. 6g–i), an inhibitor of non-canonical NF-κB signalling[26]. Notably, concomitant cGAS inactivation in the latter two genotypes was well tolerated and produced phenotypes similar to *cGAS*^{KO} cells (Extended Data Fig. 6e,f,h,i). The observation that *TRAF2* inactivation in *cGAS*^{KO} cells did not improve cell viability suggests that *TRAF2* inactivation is insufficient to hyperactivate non-canonical NF-κB signalling, possibly due to redundancy of other inhibitors of non-canonical RELB. We failed to generate *RELB;cGAS*^{DKO} cells, which suggests that RELB receives other input than only from cGAS, for instance, from the dsRNA sensor PKR, even under unperturbed conditions[27].

As CIN induces RELB signalling in our model systems (Fig. 1g) and we previously found that CIN-induced TNF–NF-κB signalling can induce apoptosis through ASK–JNK signalling[28], we next investigated whether inhibition of ASK or JNK would prevent MPS1 and WEE1 inhibitor-induced cell death of *cGAS*^{KO} BT549 cells. High doses of either the ASK1 and JNK inhibitors NQDI-1 and SP600125, respectively, were toxic to wild-type and *cGAS*^{KO} cells. By contrast, lower doses of the ASK and JNK inhibitors rescued MPS1 and WEE1 inhibitor-induced cell death in *cGAS*^{KO} cells (Fig. 1k and Extended Data Fig. 6j–l), which indicates that the cell death observed in CIN-induced *cGAS*^{KO} cells involves ASK–JNK signalling.

Together, these results reveal that TNBC cells that exhibit numerical and structural CIN induced by MPS1 and WEE1 inhibitors rely on cGAS–STING–STAT3 and non-canonical NF-κB signalling to prevent STAT1-mediated and ASK–JNK-mediated cell death.

IL-6 promotes the survival of cells with CIN

To determine which factors are involved in the decreased viability of CIN-induced *cGAS*^{KO} cells, we compared differentially expressed genes between MPS1 inhibitor-treated wild-type and *cGAS*^{KO} cells. As cGAS triggers inflammatory signalling, we focused on the expression of cytokines and interleukins. Specifically, the cytokines IL-6, CXCL8

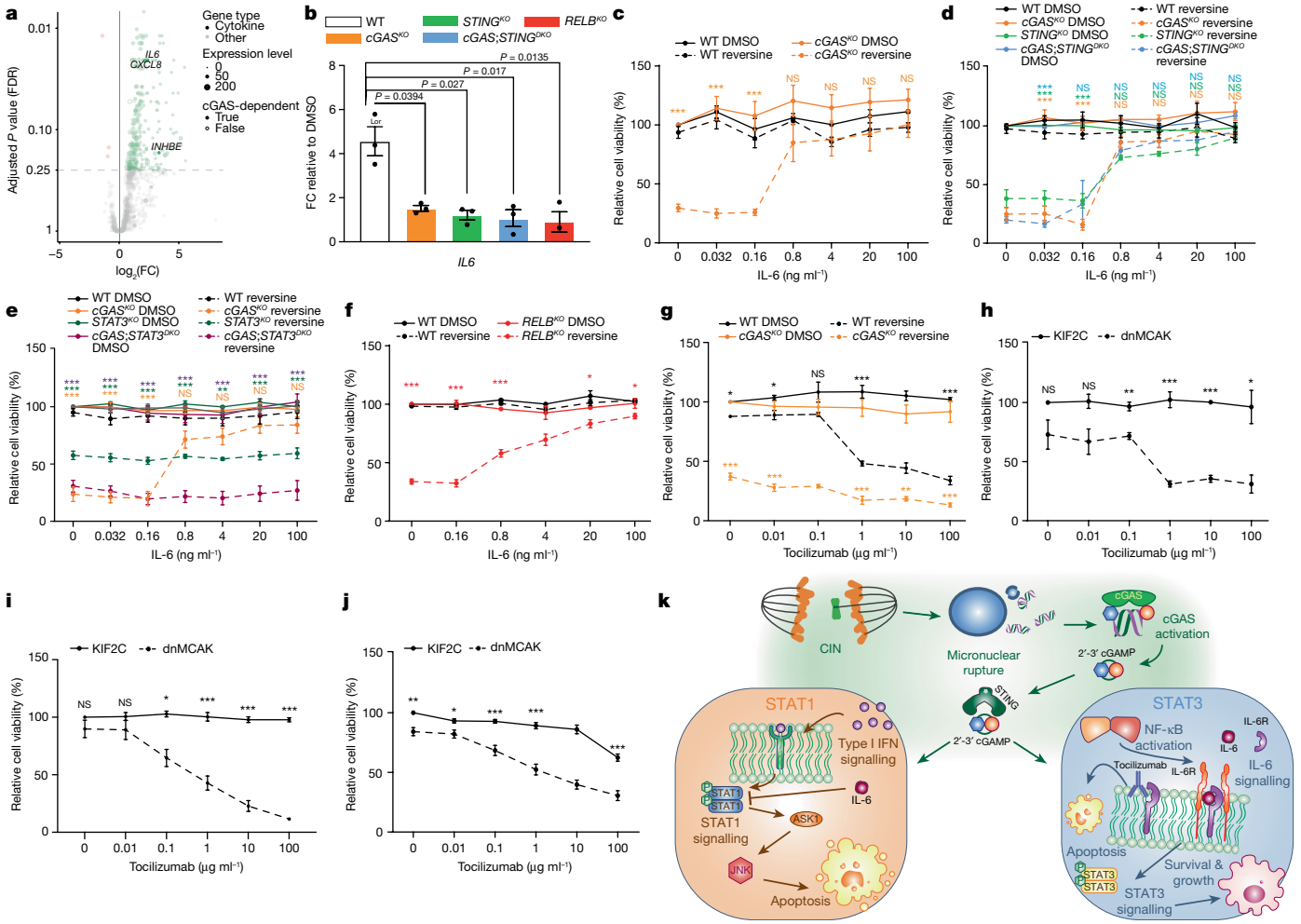

Fig. 2 | IL-6–IL-6R–STAT3 signalling induced by cGAS and STING is required for survival of TNBC cells undergoing CIN. a, Differentially expressed genes in WT BT549 cells treated with 250 nM reversine. Highlighted genes are cytokines, non-highlighted genes are other upregulated genes (for the latter, see Extended Data Fig. 4a, left). Genes for which expression depends on cGAS expression are shown as filled circles, genes for which expression is altered in both WT and *cGAS*^{KO} cells are shown as open circles. **b**, Relative *IL6* mRNA expression levels in WT, *cGAS*^{KO}, *STING*^{KO}, *cGAS;STING*^{DKO} and *RELB*^{KO} BT549 cells treated with DMSO or 250 nM reversine for 48 h. **c**–**f**, Cell viabilities of the following DMSO-treated or reversine-treated (250 nM) BT549 cells across a range of IL-6 concentrations: WT and *cGAS*^{KO} BT549 cells (**c**); WT, *cGAS*^{KO}, *STING*^{KO} and *cGAS;STING*^{DKO} (**d**); WT, *cGAS*^{KO}, *STAT3*^{KO} and *cGAS;STAT3*^{DKO} (**e**); and WT versus *RELB*^{KO} (**f**). **g**, Cell viability of DMSO- or 250 nM reversine-treated WT or *cGAS*^{KO} BT549 cells across a range of tocilizumab concentrations. **h**, Cell viabilities of BT549 cells expressing KIF2C (CIN^{low}) or dnMCAK (CIN^{high}) across a range of tocilizumab concentrations. **i**, Cell viabilities of MDA-MB-231 cells expressing KIF2C (CIN^{low}) or dnMCAK (CIN^{high}) across a range of tocilizumab concentrations. **j**, Cell viabilities of 4T1 cells expressing KIF2C (CIN^{low}) or dnMCAK (CIN^{high}) across a range of tocilizumab concentrations. **k**, Schematic representation of how cGAS drives an inflammatory response through STING, IL-6, IL-6R and STAT3 following CIN. Error bars in **b**–**j** represent the s.e.m., $n = 5$ biological replicates (**c**,**g**), $n = 4$ biological replicates (**d**,**e**), $n = 3$ biological replicates (**b**,**f**,**h**–**j**). Significance was tested with two-sided *t*-test. $^{*}P < 0.05$, $^{**}P < 0.01$, $^{***}P < 0.005$ (**c**–**j**). Exact *P* values are specified in the source data. Cells were treated for 72 h (**c**–**f**) or 96 h (**g**–**j**).

(also known as IL-8) and INHBE were upregulated in a cGAS-dependent manner following MPS1 inhibition (Fig. 2a and Extended Data Fig. 4). We followed up on IL-6 as this is a known activator of STAT3 signalling[29]. Quantitative PCR (qPCR) showed that *IL6* is upregulated following drug-induced CIN and depended on cGAS, STING and RELB (Fig. 2b and Extended Data Fig. 7a).

To determine whether cGAS-mediated IL-6 induction is required for survival after drug-induced CIN, wild-type and *cGAS*^{KO} BT549 cells in which we induced CIN were supplemented with increasing concentrations of recombinant human IL-6. Concentrations from 0.8 ng ml^{-1} of recombinant IL-6 restored the viability of MPS1 and WEE1-inhibited *cGAS*^{KO} cells without affecting the viability of mock-treated *cGAS*^{KO} or wild-type cells (Fig. 2c and Extended Data Fig. 7b,c). Lentiviral overexpression of IL-6 similarly rescued the viability of *cGAS*^{KO} cells following induction of CIN (Extended Data Fig. 7d,e). Mouse recombinant IL-6 also restored the viability of *cGas*^{KO} 4T1 cells treated with MPS1 or WEE1 inhibitors (Extended Data Fig. 7f,g). In contrast to MPS1 inhibition, the observed rescue of WEE1 inhibitor-induced cytotoxicity was partial in all conditions, which is probably due to consequences of replication stress beyond mitotic abnormalities (Extended Data Fig. 1f).

IL-6 supplementation also rescued the loss of viability of *STING*^{KO} cells (Fig. 2d and Extended Data Fig. 7h), but had no effect on *STAT3*^{KO} or *cGAS;STAT3*^{DKO} BT549 cells treated with MPS1 or WEE1 inhibitors (Fig. 2e and Extended Data Fig. 7i). These findings confirm that IL-6 operates downstream of cGAS–STING and upstream of STAT3. Similarly, supplementation of IL-6 restored the cell viability of *RELB*^{KO} BT549 cells with drug-induced CIN; however, in this genetic background, higher concentrations (about 20 ng ml^{-1}) were required to restore viability (Fig. 2f and Extended Data Fig. 7j). This observation suggests that RELB operates upstream of STAT3 but receives additional inputs besides cGAS to trigger IL-6 expression. We also tested whether IFNα (IFNA2), another STAT signalling cytokine[30], could rescue CIN-induced

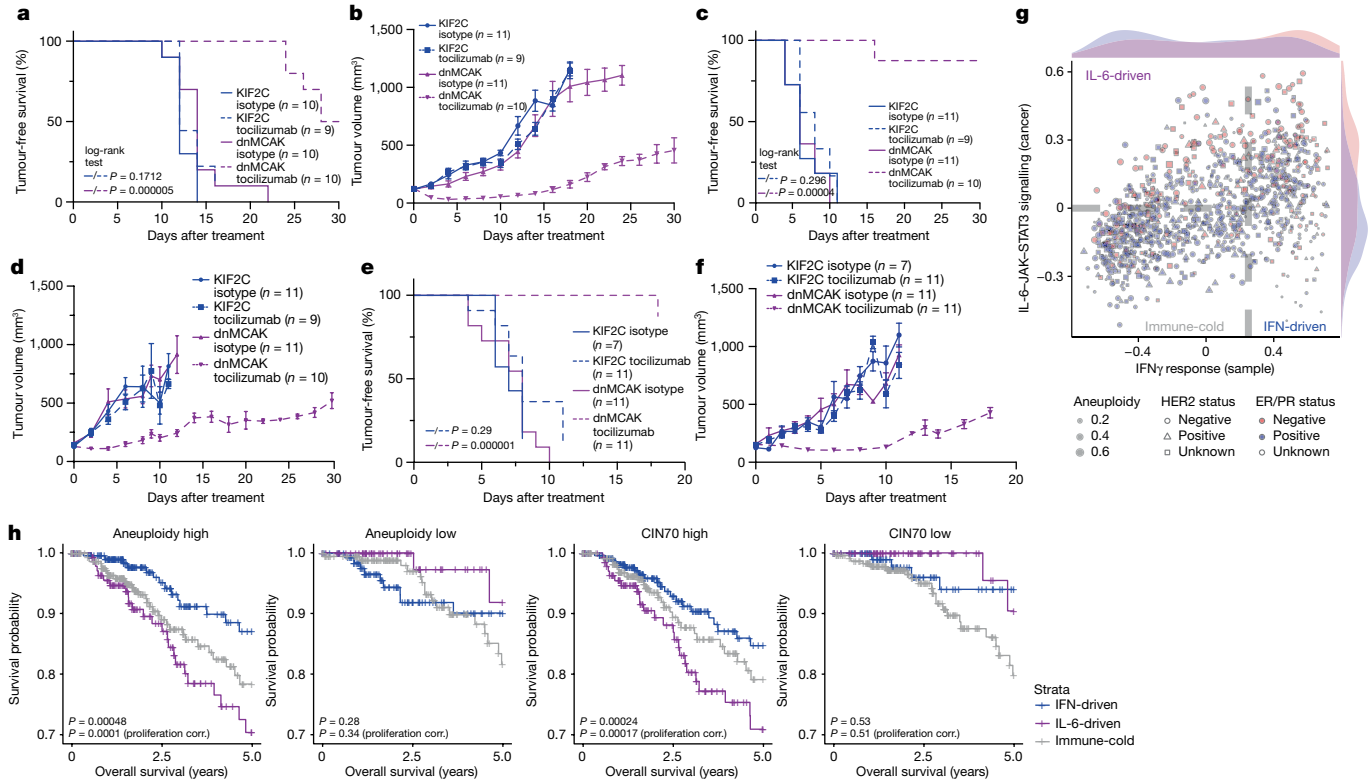

Fig. 3 | Inhibition of IL-6R impairs the growth of CIN-induced TNBC tumours. a, Tumour-free survival of immunodeficient NSG mice xenografted with MDA-MB-231 KIF2C cells (CIN^{low}) or MDA-MB-231 dnMCAK cells (CIN^{high}) treated with isotype control or tocilizumab and followed-up for 30 days. **b**, Average tumour growth in immunocompromised mice transplanted with MDA-MB-231 KIF2C cells (CIN^{low}) or MDA-MB-231 dnMCAK cells (CIN^{high}) treated with isotype control or tocilizumab. **c**, Tumour-free survival of immunocompromised mice transplanted with 4T1 KIF2C cells (CIN^{low}) or 4T1 dnMCAK cells (CIN^{high}) treated with isotype control or tocilizumab. **d**, Average tumour growth in immunocompromised mice transplanted with 4T1 KIF2C cells (CIN^{low}) or 4T1 dnMCAK cells (CIN^{high}) treated with isotype control or tocilizumab. **e**, Tumour-free survival of immunocompetent Balb/c mice transplanted with 4T1 KIF2C cells (CIN^{low}) or 4T1 dnMCAK cells (CIN^{high}) treated with isotype control or tocilizumab. **f**, Average tumour growth in immunocompetent Balb/c mice transplanted with 4T1 KIF2C cells (CIN^{low}) or 4T1 dnMCAK cells (CIN^{high}) treated with isotype control or tocilizumab. For **a**–**f**, tumours are defined as masses >500 mm^3. Significance was tested with log-rank test. **g**, TCGA breast cancer samples scored for IFN-responsive gene activity (*x* axis) versus IL-6–STAT3 signalling gene activity (*y* axis), including tumour aneuploidy (symbol size), hormone receptor status (colour) and HER2 status (shape). Grey dashed lines indicate our partition in immune-cold, IFN-driven and IL-6-driven groups. Shaded regions indicate the density of the hormone receptor status on the respective axes. ER/PR, oestrogen receptor/progesterone receptor. **h**, Patient survival stratified by aneuploidy and CIN status (CIN70) for breast tumours, with tumour partitions in **g**. *P* value indicates the difference between IL-6–STAT3 and IFN groups in a multivariate Cox regression.

cell death of $cGAS^{KO}$ cells. Recombinant IFNA2 improved cell viability of reversine-treated or AZD1775-treated $cGAS^{KO}$ cells, but not $STAT3^{KO}$ or $cGAS;STAT3^{DKO}$ cells within a concentration range of 2–10 ng ml^{-1}. Higher IFNA2 concentrations, however, decreased viability, particularly of $cGAS^{KO}$ cells (Extended Data Fig. 7k–n). It is possible that higher IFNA2 concentrations hyperactivate STAT1 (ref. [31]) and therefore promote cell death in line with our earlier observations (Extended Data Fig. 5g). This result suggests that both IFN and NF-κB signalling are involved in protecting cells against CIN-induced cell death. IFN modulates both cell-death-promoting STAT1 and protective STAT3, whereas IL-6 only activates the latter, thus producing a stronger rescue phenotype. We conclude that inhibition of MPS1 and WEE1 induces the expression of IL-6 in a cGAS–STING-dependent manner, upstream of STAT3, and that TNBC cells rely on IL-6 expression under these circumstances for survival.

IL-6R inhibition sensitizes cells to CIN

As TNBC cells rely on IL-6 expression for survival when exposed to drugs that induce CIN, we next tested whether pharmacological inhibition of IL-6 signalling in TNBC cells would increase their sensitivity to CIN. Treatment of BT549 cells with the IL-6R inhibitor tocilizumab significantly reduced the viability of MPS1 inhibitor-treated BT549 cells, without affecting control cells (Fig. 2g). $cGAS^{KO}$ BT549 cells were minimally sensitive to tocilizumab treatment (Fig. 2g), which confirms that IL-6 pro-survival signalling is near-completely abrogated in $cGAS^{KO}$ BT549 cells. Notably, MPS1 inhibitor-induced CIN (Extended Data Fig. 8a) produced highly similar phenotypes in three additional human TNBC cell lines (MDA-MB-231, MDA-MB-436 and E0771), but not in untransformed MCF10A cells (Extended Data Fig. 8b–e).

To determine whether chronic CIN also sensitizes cancer cells to tocilizumab, we introduced KIF2C and dnMCAK into BT549 and MDA-MB-231 cells and confirmed CIN rates by time-lapse microscopy (Extended Data Fig. 8f,g). We then exposed BT549, MDA-MB-231 and 4T1 cells expressing either KIF2C or dnMCAK to tocilizumab. The viability of KIF2C-expressing BT549, MDA-MB-231 and 4T1 (CIN^{low}) cells was unaffected by this treatment, whereas their dnMCAK-expressing (CIN^{high}) counterparts displayed a substantial reduction in viability (Fig. 2h–j) and proliferation (Extended Data Fig. 8h–j) following tocilizumab treatment at similar concentrations observed for cells treated with CIN-inducing drugs. We conclude that inhibition of the cGAS–STING–IL-6–STAT3 axis is toxic to TNBC cells with acute and chronic CIN, but not to untransformed MCF10A cells or cells without a CIN phenotype (Fig. 2k).

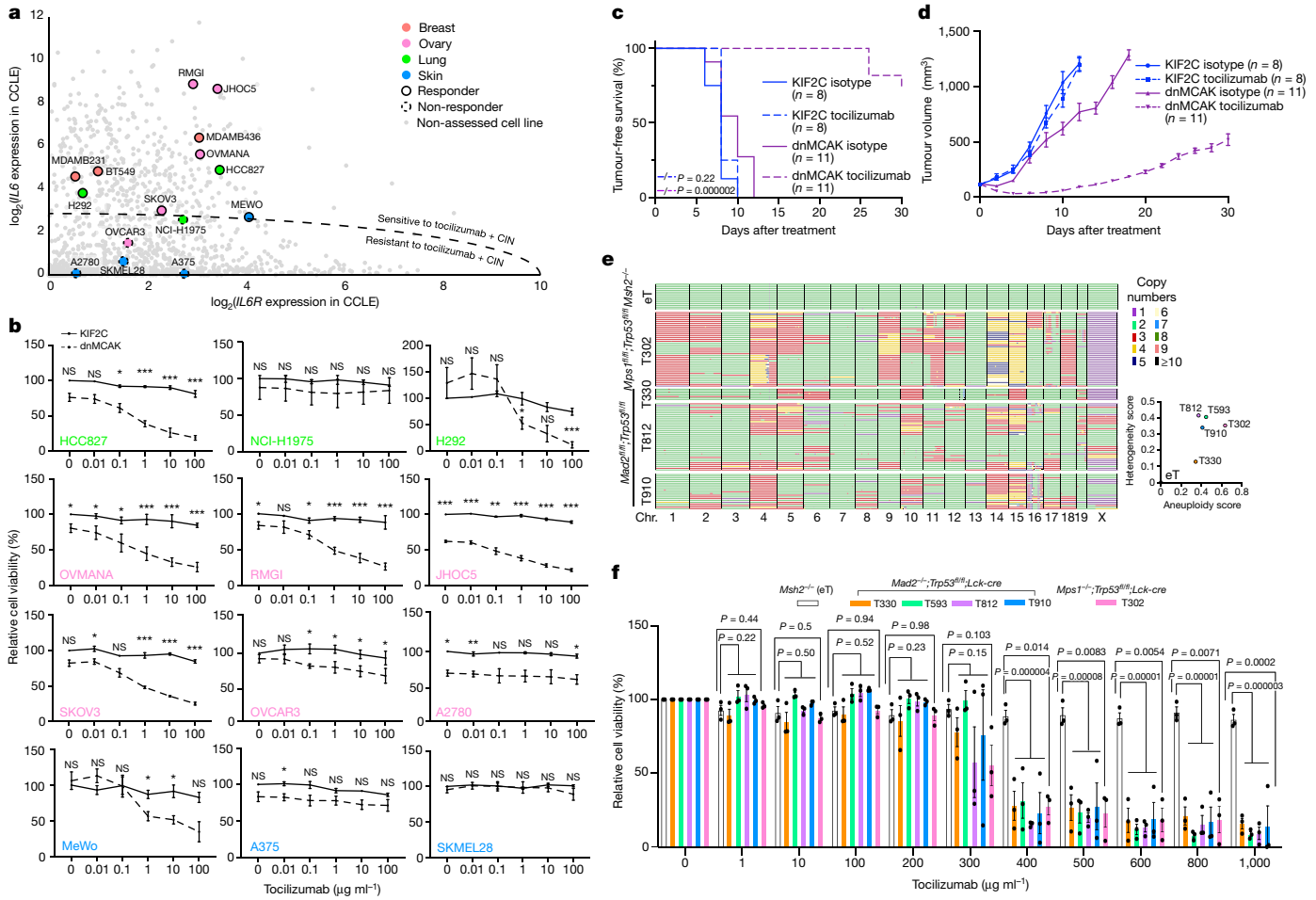

Fig. 4 | IL-6 signalling is required for cancer cells that display acute or chronic CIN in vitro and in vivo observed across cancer types. **a**, DepMap-annotated mRNA expression data for *IL6* and *IL6R* for CCLE-included cancer cell lines. Cell lines that were included in this study are highlighted. Cell lines above the dashed line are predicted to be sensitive to tocilizumab in combination with acute or chronic CIN based on our findings. **b**, Relative cell viability of KIF2C (CIN^{low}) or dnMCAK (CIN^{high}) cells across a range of tocilizumab concentrations. Top, lung cancer cell lines. Middle, ovarian cancer cell lines. Bottom, skin cancer cell lines. **c**, Tumour-free survival of immunodeficient NSG mice transplanted with HCC827 KIF2C cells (CIN^{low}) or HCC827 dnMCAK cells (CIN^{high}) treated with isotype control or tocilizumab and followed-up for 30 days. Tumours are defined as masses >500 mm^3. Significance tested with log-rank test. **d**, Average tumour growth in immunodeficient NSG mice transplanted with HCC827 KIF2C cells (CIN^{low}) or HCC827 dnMCAK cells (CIN^{high}) treated with isotype control (KIF2C, $n = 8$; dnMCAK, $n = 11$ tumours) or tocilizumab (KIF2C, $n = 8$; dnMCAK, $n = 11$ tumours). **e**, Chromosome copy number heatmaps for $Msh2^{-/-}$ (euploid T-ALL; eT), $Mad2^{fl/fl}$;$Trp53^{fl/fl}$;*Lck-cre* ($Mad2^{fl/fl}$;$Trp53^{fl/fl}$) and $Mps1^{fl/fl}$;$Trp53^{fl/fl}$;*Lck-cre* ($Mps1^{fl/fl}$;$Trp53^{fl/fl}$) T-ALLs determined by shallow single-cell whole-genome sequencing. Each line in the heatmap represents the karyotype of a single cell, and colours represent the copy number state for each chromosome (fragment). Heterogeneity and aneuploidy scores are plotted on the right. **f**, Relative cell numbers of $Msh2^{-/-}$ (eT), $Mad2^{fl/fl}$;$Trp53^{fl/fl}$;*Lck-cre* (T330, T593, T812 and T910) and $Mps1^{fl/fl}$;$Trp53^{fl/fl}$;*Lck-cre* (T302) T-ALL primary cultures treated with different concentrations of tocilizumab or isotype control. Error bars in **b** and **f** represent the s.e.m., $n = 3$ biological replicates. Significance tested with two-sided *t*-test (**b**,**f**). $^*P < 0.05$, $^{**}P < 0.01$, $^{***}P < 0.0005$. Exact *P* values are specified in the source data.

Tocilizumab blocks the growth of CIN tumours

To validate our findings in vivo, we xenografted MDA-MB-213 cells expressing KIF2C (CIN^{low}) or dnMCAK (CIN^{high}) into immunocompromised mice and treated mice with tocilizumab or an isotype IgG control. When treated with isotype IgG, tumour growth kinetics were identical for mice harbouring CIN^{low}KIF2C or CIN^{high}dnMCAK tumours (Fig. 3a,b and Extended Data Fig. 8k). By contrast, tocilizumab treatment largely impaired the growth of CIN^{high}dnMCAK tumours, but not of CIN^{low}KIF2C tumours (Fig. 3a,b and Extended Data Fig. 8k), which indicates that tocilizumab can prevent the outgrowth of tumours with CIN in vivo. Immunohistochemistry of tumours showed that dnMCAK induced the expression and perinuclear localization of STING and the phosphorylation of $STAT1^{Y701}$, which confirms that cGAS–STING signalling was induced by dnMCAK-mediated CIN (Extended Data Fig. 8l–p).

Although our results largely pointed towards a cell-intrinsic phenotype, we evaluated cell-extrinsic (that is, immune-regulated) effects of tocilizumab. Using mouse 4T1 cells in immunocompromised athymic mice and in immune-proficient Balb/c mice, we observed that tocilizumab treatment significantly delayed tumour progression of only CIN^{high}dnMCAK 4T1 tumours in both immune-deficient and immune-proficient backgrounds (Fig. 3c–f and Extended Data Fig. 8q–r). We therefore conclude that tocilizumab specifically prevents the in vivo outgrowth of human and mouse TNBC cells with CIN in a cell-intrinsic and potentially a cell-extrinsic manner.

Correlation between IL-6 and CIN in cancer

To determine the importance of active IL-6 signalling with respect to human primary breast cancers, we performed correlations for aneuploidy, CIN (as determined by the CIN70 signature[32]), cGAS, IL-6 and

IL-6R expression in the cohort from The Cancer Genome Atlas (TCGA) (Extended Data Fig. 9). We only included primary tumours to exclude the beneficial effects that cGAS has on metastasis[5]. Tumours with high cGAS expression showed high aneuploidy and CIN as well as IL-6 and IL-6R expression and their transcriptional footprints. This strongly suggests that particularly CIN^{high} primary breast tumours activate cGAS–IL-6–IL-6R signalling. We then split the cohort on the basis of inferred cancer-specific IL-6–STAT3 activity and total IFN activity (Fig. 3g). Tumours with high aneuploidy and CIN with activated IL-6 signalling showed overall decreased survival compared with tumours with high overall inflammation. Tumours with low aneuploidy and CIN did not show a difference in survival in this comparison (Fig. 3h). We conclude that human breast cancers, in particular TNBCs, frequently activate cGAS–IL-6–IL-6R signalling and that this leads to poor patient survival.

IL-6 and IL-6R predict response to tocilizumab

As our experiments above showed that IL-6–STAT3 signalling is activated in TNBC cells with CIN and that they have increased survival, we next tested whether cancer cell lines that express high levels of IL-6R are functionally different from cancer cell lines that express low levels of IL-6R. To assess this, we first analysed gene essentiality in relation to IL-6R expression in cell lines using the DepMap database[33,34] (Extended Data Fig. 10a). There was a positive correlation between IL-6R levels and essentiality of genes (that is, high levels of IL-6R are associated with less gene dependency) involved in DNA repair, chromosome maintenance and the mitotic spindle assembly checkpoint. These genes become less essential in Cancer Cell Line Encyclopedia (CCLE)-included cancer cell lines that overexpress IL-6R. This suggests that CCLE-included cancer cell lines with high IL-6R levels are able to better regulate CIN across multiple cancer types.

To further test this hypothesis, we selected a panel of non-TNBC cell lines representing several cancer types (ovarian cancer, lung cancer and skin cancer) that are known to express different levels of IL-6 and IL-6R (Fig. 4a), which we confirmed in our cells by qPCR (Extended Data Fig. 10b). We then induced chronic CIN through expression of dnMCAK or acute CIN through MPS1 inhibition (Extended Data Fig. 10c) and compared cell viability to control-treated cells (KIF2C or dimethyl sulfoxide (DMSO), respectively) following treatment with increasing concentrations of tocilizumab. Cell lines expressing high levels of IL-6 and/or IL-6R were susceptible to tocilizumab-mediated death when exposed to either chronic or acute CIN (Fig. 4b, Extended Data Fig. 10d,) whereas cell lines that expressed low levels of IL-6 and/or IL-6R were resistant to tocilizumab treatment up to doses of 1 mg ml^{-1} (Extended Data Fig. 10e).

We next tested the relevance of these findings in patient tumours of the same tissues. Similar to TNBC cells, aneuploid lung cancer and ovarian cancer that display high IL-6–STAT3 activity were associated with overall decreased patient survival compared with tumours with low IL-6–STAT3 activity (Extended Data Fig. 10f). This correlation did not hold for skin cancers (Extended Data Fig. 10f), which may be explained by the generally low expression levels of cGAS and IL-6 in these cancers (Extended Data Fig. 10g). Moreover, two out of three tested skin cancer cell lines expressed low levels of IL-6 and are therefore not sensitive to tocilizumab in combination with CIN (Fig. 4a,b and Extended Data Fig. 10b, d).

We also confirmed whether our findings in other cancer types are true in vivo. For this, we xenografted CIN^{low}KIF2C or CIN^{high}dnMCAK HCC827 lung cancer cells into immunocompromised mice. As observed for human MDA-MB-231 and mouse 4T1 TNBC cells, tocilizumab treatment significantly delayed HCC827 tumour growth, but only in a CIN^{high} background (Fig. 4c,d and Extended Data Fig. 10h). Finally, we tested our hypothesis in primary cultures derived from genetically engineered mouse models for CIN-induced acute T cell lymphoma (T-ALL). Specifically, we established four primary T-ALL cultures from *Mad2*$^{fl/fl}$;*Trp53*$^{fl/fl}$;*Lck-cre* mice[35] and one primary T-ALL culture from *Mps1*$^{fl/fl}$;*Trp53*$^{fl/fl}$;*Lck-cre* mice[36]. As a euploid control, we cultured primary T-ALL cells from *Msh2*$^{-/-}$ mice[37]. We quantified CIN by single-cell whole-genome sequencing[38,39], which confirmed that *Mps1*$^{fl/fl}$;*Trp53*$^{fl/fl}$;*Lck-cre* and *Mad2*$^{fl/fl}$;*Trp53*$^{fl/fl}$;*Lck-cre* mice displayed high-grade aneuploidy and karyotype heterogeneity in line with chronic CIN (Fig. 4e; single-cell whole-genome sequencing data for T593 was previously published[40]). By contrast, *Msh2*$^{-/-}$ T-ALL cells were completely euploid (Fig. 4e). When we exposed all primary T-ALL cultures to increasing concentrations of tocilizumab, all cultures, except for *Msh2*$^{-/-}$ T-ALL cultures, were susceptible to tocilizumab-mediated death (Fig. 4f), which correlated well with IL-6 and IL-6R expression (Extended Data Fig. 10i). We therefore conclude that tocilizumab selectively kills cancer cells of various lineages with an acute or chronic CIN phenotype in vitro and in vivo, but only if IL-6–STAT3 signalling is activated, for example, through increased expression of IL-6 and/or IL-6R.

Altogether, our findings reveal that cells that display CIN rely on a cGAS-mediated inflammatory response for their survival. This offers an explanation for why cGAS and STING are rarely inactivated in primary cancers[4,5] and complements the finding that a cGAS–STING inflammatory response induced by genomic instability promotes tumorigenesis[41]. Our work also exposes a targetable vulnerability for cells that display CIN, as IL-6 and its receptor IL-6R are pivotal components of this signalling cascade. This was confirmed across cancer types using the IL-6R inhibitor tocilizumab in mouse and human cell lines, in vitro and in vivo. Our findings furthermore suggest that drug-induced CIN in combination with tocilizumab could be an effective treatment for cancers that display activated IL-6 signalling. Repurposing this clinically used drug[42], possibly in combination with STING agonists[43] or drugs that induce CIN such as paclitaxel[44,45] or vincristine[44], could provide a strategy to treat cancers that rely on this signalling and are associated with poor prognosis.

Online content

Any methods, additional references, Nature Research reporting summaries, source data, extended data, supplementary information, acknowledgements, peer review information; details of author contributions and competing interests; and statements of data and code availability are available at https://doi.org/10.1038/s41586-022-04847-2.

1. Sansregret, L., Vanhaesebroeck, B. & Swanton, C. Determinants and clinical implications of chromosomal instability in cancer. *Nat. Rev. Clin. Oncol.* **15**, 139–150 (2018).
2. MacKenzie, K. J. et al. CGAS surveillance of micronuclei links genome instability to innate immunity. *Nature* **548**, 461–465 (2017).
3. Harding, S. M. et al. Mitotic progression following DNA damage enables pattern recognition within micronuclei. *Nature* **548**, 466–470 (2017).
4. Bakhoum, S. F. & Cantley, L. C. The multifaceted role of chromosomal instability in cancer and its microenvironment. *Cell* **174**, 1347–1360 (2018).
5. Bakhoum, S. F. et al. Chromosomal instability drives metastasis through a cytosolic DNA response. *Nature* **553**, 467–472 (2018).
6. Ben-David, U. & Amon, A. Context is everything: aneuploidy in cancer. *Nat. Rev. Genet.* **21**, 44–62 (2020).
7. Zhou, L., Jilderda, L. J. & Foijer, F. Exploiting aneuploidy-imposed stresses and coping mechanisms to battle cancer. *Open Biol.* **10**, 200148 (2020).
8. Santaguida, S. et al. Chromosome mis-segregation generates cell-cycle-arrested cells with complex karyotypes that are eliminated by the immune system. *Dev. Cell* **41**, 638–651.e5 (2017).
9. Hirai, H. et al. Small-molecule inhibition of Wee1 kinase by MK-1775 selectively sensitizes p53-deficient tumor cells to DNA-damaging agents. *Mol. Cancer Ther.* **8**, 2992–3000 (2009).
10. Heijink, A. M. et al. A haploid genetic screen identifies the G_1/S regulatory machinery as a determinant of Wee1 inhibitor sensitivity. *Proc. Natl Acad. Sci. USA* **112**, 15160–15165 (2015).
11. Pépin, G. & Gantier, M. Assessing the cGAS–cGAMP–STING activity of cancer cells. *Methods Mol. Biol.* **1725**, 257–266 (2018).
12. Parkes, E. E. et al. The clinical and molecular significance associated with STING signaling in breast cancer. *NPJ Breast Cancer* **7**, 81 (2021).
13. Dixon, C. R. et al. STING nuclear partners contribute to innate immune signaling responses. *iScience* **24**, 103055 (2021).
14. Basit, A. et al. The cGAS/STING/TBK1/IRF3 innate immunity pathway maintains chromosomal stability through regulation of p21 levels. *Exp. Mol. Med.* **52**, 643–657 (2020).

15. Zhong, L. et al. Phosphorylation of cGAS by CDK1 impairs self-DNA sensing in mitosis. *Cell Discov.* **6**, 26 (2020).
16. Suter, M. A. et al. cGAS–STING cytosolic DNA sensing pathway is suppressed by JAK2–STAT3 in tumor cells. *Sci. Rep.* **11**, 7243 (2021).
17. Vincent, J. et al. Small molecule inhibition of cGAS reduces interferon expression in primary macrophages from autoimmune mice. *Nat. Commun.* **8**, 750 (2017).
18. Manning, A. L. et al. The kinesin-13 proteins Kif2a, Kif2b, and Kif2c/MCAK have distinct roles during mitosis in human cells. *Mol. Biol. Cell* **18**, 2970–2979 (2007).
19. Pulaski, B. A. & Ostrand-Rosenberg, S. Mouse 4T1 breast tumor model. *Curr. Protoc. Immunol.* https://doi.org/10.1002/0471142735.im2002s39 (2000).
20. Parkes, E. E. et al. Activation of STING-dependent innate immune signaling by S-phase-specific DNA damage in breast cancer. *J. Natl Cancer Inst.* **109**, djw199 (2016).
21. Orr, B., Talje, L., Liu, Z., Kwok, B. H. & Compton, D. A. Adaptive resistance to an inhibitor of chromosomal instability in human cancer cells. *Cell Rep.* **17**, 1755–1763 (2016).
22. Avalle, L., Pensa, S., Regis, G., Novelli, F. & Poli, V. STAT1 and STAT3 in tumorigenesis: a matter of balance. *JAKSTAT* **1**, 65–72 (2012).
23. Hui, K. P. Y. et al. Highly pathogenic avian influenza H5N1 virus delays apoptotic responses via activation of STAT3. *Sci. Rep.* **6**, 28593 (2016).
24. Carter, L. et al. Molecular analysis of circulating tumor cells identifies distinct copy-number profiles in patients with chemosensitive and chemorefractory small-cell lung cancer. *Nat. Med.* **23**, 114–119 (2016).
25. Senftleben, U. et al. Activation by IKKα of a second, evolutionary conserved, NF-κB signaling pathway. *Science* **293**, 1495–1499 (2001).
26. Chen, S.-J., Huang, S.-S. & Chang, N.-S. Role of WWOX and NF-κB in lung cancer progression. *Transl. Resp. Med.* **1**, 15 (2013).
27. Zamanian-Daryoush, M., Mogensen, T. H., DiDonato, J. A. & Williams, B. R. G. NF-κB activation by double-stranded-RNA-activated protein kinase (PKR) is mediated through NF-κB-inducing kinase and IκB kinase. *Mol. Cell. Biol.* **20**, 1278–1290 (2000).
28. Heijink, A. M. et al. BRCA2 deficiency instigates cGAS-mediated inflammatory signaling and confers sensitivity to tumor necrosis factor-α-mediated cytotoxicity. *Nat. Commun.* **10**, 100 (2019).
29. Johnson, D. E., O'Keefe, R. A. & Grandis, J. R. Targeting the IL-6/JAK/STAT3 signalling axis in cancer. *Nat. Rev. Clin. Oncol.* **15**, 234–248 (2018).
30. Horvath, C. M. The Jak–STAT pathway stimulated by interferon α or interferon β. *Sci. STKE* **2004**, tr10 (2004).
31. Bromberg, J. F., Horvath, C. M., Wen, Z., Schreiber, R. D. & Darnell, J. E. Transcriptionally active Stat1 is required for the antiproliferative effects of both interferon alpha and interferon gamma. *Proc. Natl Acad. Sci. USA* **93**, 7673–7678 (1996).
32. Carter, S. L., Eklund, A. C., Kohane, I. S., Harris, L. N. & Szallasi, Z. A signature of chromosomal instability inferred from gene expression profiles predicts clinical outcome in multiple human cancers. *Nat. Genet.* **38**, 1043–1048 (2006).
33. Meyers, R. M. et al. Computational correction of copy number effect improves specificity of CRISPR–Cas9 essentiality screens in cancer cells. *Nat. Genet.* **49**, 1779–1784 (2017).
34. Tsherniak, A. et al. Defining a cancer dependency map. *Cell* **170**, 564–576 (2017).
35. Foijer, F. et al. Deletion of the MAD2L1 spindle assembly checkpoint gene is tolerated in mouse models of acute T-cell lymphoma and hepatocellular carcinoma. *eLife* **6**, e20873 (2017).
36. Foijer, F. et al. Chromosome instability induced by *Mps1* and *p53* mutation generates aggressive lymphomas exhibiting aneuploidy-induced stress. *Proc. Natl Acad. Sci. USA* **111**, 13427–13432 (2014).
37. de Wind, N., Dekker, M., Berns, A., Radman, M. & te Riele, H. Inactivation of the mouse *Msh2* gene results in mismatch repair deficiency, methylation tolerance, hyperrecombination, and predisposition to cancer. *Cell* **82**, 321–330 (1995).
38. Bakker, B. et al. Single-cell sequencing reveals karyotype heterogeneity in murine and human malignancies. *Genome Biol.* **17**, 115 (2016).
39. van den Bos, H. et al. Quantification of aneuploidy in mammalian systems. *Methods Mol. Biol.* **1896**, 159–190 (2019).
40. Shoshani, O. et al. Transient genomic instability drives tumorigenesis through accelerated clonal evolution. *Genes Dev.* **35**, 1093–1109 (2021).
41. Pozo, F. M. et al. MYO10 drives genomic instability and inflammation in cancer. *Sci. Adv.* **7**, eabg6908 (2021).
42. LJ, S. Tocilizumab: a review in rheumatoid arthritis. *Drugs* **77**, 1865–1879 (2017).
43. Decout, A., Katz, J. D., Venkatraman, S. & Ablasser, A. The cGAS–STING pathway as a therapeutic target in inflammatory diseases. *Nat. Rev. Immunol.* **21**, 548–569 (2021).
44. Jones, V. S. et al. Cytokines in cancer drug resistance: cues to new therapeutic strategies. *Biochim. Biophys. Acta* **1865**, 255–265 (2016).
45. Duan, Z., Lamendola, D. E., Penson, R. T., Kronish, K. M. & Seiden, M. V. Overexpression of IL-6 but not IL-8 increases paclitaxel resistance of U-2OS human osteosarcoma cells. *Cytokine* **17**, 234–242 (2002).

Methods

Data reporting

No statistical methods were used to predetermine sample sizes. The investigators were not blinded to allocation during experiments and outcome assessment.

Data deposition

RNA sequencing data have been deposited at ArrayExpress under the accession number E-MTAB-10923. Shallow single-cell whole-genome sequencing data have been deposited at the European Nucleotide Archive under the accession number PRJEB49800.

Cell culture

BT549 (American Type Culture Collection (ATCC), HTB-122), 4T1 (ATCC, CRL-2359), E0771 (ATCC, CRL-3461), HCC827 (ATCC, CRL-2868), NCI-H1975 (ATCC, CRL-5908), H292 (ATCC, CRL-1848), OVMANA (JCRB Cell Bank, JCRB1045), RMG-I (JCRB Cell Bank, JCRB0172), JHOC5 (RIKEN Cell Bank, RCB1520), SKOV3 (ATCC, HTB-77), OVCAR3 (ATCC, HTB-161), A2780 (Sigma Aldrich, 93112519), MeWo (ATCC, HTB-65), A375 (ATCC, CRL-1619) and SKMEL28 (ATCC, HTB-72) cell lines were cultured in RPMI 1640 medium with GlutaMAX supplement (Thermo Fisher), 10% FBS (Thermo Fisher Scientific) and 100 U ml^{-1} penicillin and streptomycin (P/S; Thermo Fisher). MDA-MB-231 (ATCC, CRM-TB-26), MDA-MB-436 (ATCC, HTB-130), Phoenix Ampho (ATCC, CRL-3213) and 293T (ATCC, CRL-3216) cell lines were cultured in DMEM with 10% FBS and 100 U ml^{-1} P/S. MCF10A (ATCC, CRL-10317) cells were cultured in DMEM/F-12 supplemented with 5% horse serum (Invitrogen), 50 U μl^{-1} P/S, 100 ng ml^{-1} cholera toxin (Sigma), 20 ng ml^{-1} epidermal growth factor (Peprotech), 10 μg ml^{-1} insulin (Sigma) and 500 ng ml^{-1} hydrocortisone (Sigma). All cells were grown at 37 °C and 5% CO_2 in a humidified incubator. Cells were routinely checked for mycoplasma infection and tested negative. The identity and purity of cell lines were validated using the short tandem repeat method by the vendors.

Generation of knockout cell lines using CRISPR–Cas9

CRISPR guide RNAs targeting the coding sequence of the relevant human or mouse genes (Supplementary Table 1) were cloned into a Cas9 plasmid using BbsI (NEB). The pSpCas9(BB)-2A-Puro V2.0 (PX459) was a gift from F. Zhang[46] (Addgene, plasmid 62988). To generate knockouts for genes of interest, BT549 and 4T1 cells were transfected with the indicated guide RNA plasmids (2 μg) using FuGene (Promega) according to the manufacturer's protocols. After 48 h of transfection, cells were selected with puromycin (Invivogen, 1 μg ml^{-1} for BT549 and 2 μg ml^{-1} for 4T1) for 48 h before validating the knockouts by immunoblotting. Single clones for indicated knockouts were generated from single cells derived from a polyclonal population and seeded into a 96-well plate. Individual clones were grown and validated by immunoblotting.

Immunoblotting

Cells were lysed in ELB (150 mM NaCl, 50 mM HEPES pH 7.5, 5 mM EDTA and 0.1% NP-40) supplemented with protease (Roche) and phosphatase inhibitors (Sigma Aldrich). Protein lysates were then mixed with a 5× sample buffer (50% glycerol, 10% SDS, 0.5 M DTT and 250 mM Tris pH 6.8) and boiled for 5 min at 98 °C. Samples were separated on SDS–PAGE and transferred onto a polyvinylidene difluoride membrane (Millipore). Information on primary and secondary antibodies is provided in Supplementary Table 2. We used two different detection methods depending on the primary antibody used: infrared fluorescence (LiCor Odyssey) or chemiluminescence (as indicated in Supplementary Table 2). Membranes were blocked for 30 min at room temperature in Odyssey blocking buffer (LiCor) diluted 1:1 with TBS (19 mM Tris base, 137 mM NaCl and 2.7 mM KCl) or 5% BSA (Sigma Aldrich) in TBS for infrared fluorescence or chemiluminescence detection, respectively. Blots were incubated with primary antibodies at 4 °C overnight. Membranes were washed 3 times (5 min each) with TBS-T (TBS plus 0.1% Tween-20). Secondary antibodies (primary and secondary antibody combinations are provided in Supplementary Table 2) were incubated with the membrane for 1 h at room temperature. For infrared fluorescence, membranes were washed 3 times (5 min each) with TBS-T before detection using an Odyssey CLx scanner (LiCor). Images were visualized and analysed using ImageStudio Lite Software (LiCor). For chemiluminescence, membranes were washed 3 times (5 min each) and protein signals were visualized with Clarity Western ECL substrate (Bio-Rad) using an ImageQuant LAS 4000 scanner (GE Healthcare). Generated images were visualized and analysed using ImageJ. Uncropped immunoblot images are provided in Supplementary Fig. 1.

Vector engineering and retroviral and lentiviral transductions

To generate a constitutive human IL-6 overexpression plasmid, *IL6* from human cDNA was amplified, flanked by BamHI and EcoRI restriction sites using Phusion polymerase (NEB, M0530L) and cloned into a pLV-CMV plasmid. The pLV-CMV plasmid was generated from a pLVX plasmid (Clontech, 632164). pLV-CMV-KIF2C and pLV-CMV-dnMCAK were generated by transferring *KIF2C* or dn*MCAK* cDNA, respectively, from earlier described cDNA vectors[5] into a pLV-CMV CMV plasmid using BamHI and EcoRI (for KIF2C) or MluI (for dnMCAK). Inducible KIF2C and dnMCAK expression plasmids were generated by subcloning KIF2C and dnMCAK from pLV-CMV plasmids into a pLVX plasmid using the restriction sites BamHI and EcoRI (for KIF2C) or MluI (for dnMCAK). To generate an inducible STAT1 overexpression plasmid, *STAT1* was amplified from human cDNA, cloned into a pMiniT2.0 plasmid and then transferred into a pRetrox plasmid (Clontech) using BamHI andMluI restriction sites. To generate mutant versions of STAT1 (Y701A and Y701E), we used site-directed mutagenesis using a Q5 Site-Directed Mutagenesis kit (NEB, E0554) using pMiniT2.0-STAT1 as input. The sequence was validated by Sanger sequencing, and mutant STAT1 fragments were transferred into a pRetrox plasmid using the same cloning strategy as used for wild-type STAT1. PIGPZ–H2B–Cherry was subcloned from an existing H2B–Cherry construct using NotI and BsrGI sites. pLNCX2 H2B–GFP–T2A–CENPB–mCherry was engineered using a Gibson assembly kit (NEB) as previously described[47]. All used restriction enzymes were purchased from New England Biolabs (NEB). Primers used for cloning were designed with Snapgene software and are listed in Supplementary Table 1.

Lentiviral transductions of pIGZ H2B–Cherry, pLV-CMV human IL-6, pLV-CMV KIF2C, pLV-CMV dnMCAK, pLVX KIF2C or pLVX dnMCAK were achieved by transfecting 3 μg of the desired plasmid supplemented with the following packaging plasmids: 3 μg pSPAX2 and 1 μg pMD2.G into 293T cells. psPAX2 (Addgene plasmid, 12260) and pMD2.G (Addgene plasmid, 12259) were gifts from Prof. D. Trono (École Polytechnique Fédérale de Lausanne (EPFL)). After 48 h of transfection, the medium from 293T cells was collected, passed through a 0.45-μm filter (VWR Science) and transferred onto the target cells. To increase transduction efficiency, polybrene (Millipore) was added to a final concentration of 8 μg ml^{-1}. Retroviral transductions of pRetrox-STAT1, pRetrox-STAT1-Y701E or pRetrox-STAT1-Y701A were carried out by transfecting 3 μg of the desired plasmid into Phoenix Ampho cells. Viruses were collected and used for transduction as described for lentiviral transduction.

Quantification of cell numbers after treatment

A total of 20,000 BT549 cells, wild-type cells or different knockouts were seeded per well in 12-well plates. After 24 h, 250 nM reversine (Sigma Aldrich, R3904), 500 nM AZD1775 (Axon Medchem, 1494) or DMSO (AppliChem) was added to the respective wells (48 h for AZD1775 or 72 h for reversine). Following treatment, cells were dissociated using Tryple Express (Thermo Fisher Scientific) and counted using a TC20 automated cell counter (Bio-Rad). Cell numbers were analysed using Microsoft Excel.

MTT assays

BT549, 4T1, MDA-MB-231, MDA-MB-436, E0771, MCF10A, HCC827, NCI-H1975, H292, OVMANA, RMG-I, JHOC5, SKOV3, OVCAR3, A2780, MeWo, A375 and SKMEL28 cells (with or without genetic modifications) were plated in 96-wells plates at a density of 1,000–2,000 cells per well. After 24 h, cells were treated with the indicated concentrations of the following compounds: reversine, AZD1775, doxycycline (Sigma Aldrich, D9891), RU.521 (Invivogen, inh-ru521), tocilizumab (Roche), the ASK1 inhibitor NQDI-1 (Axon Medchem, 2179), the JNK inhibitor SP600125 (Selleck Chemicals, S1460), UMK-57 (AOBIOUS, AOB8668), 5-fluorouracil (Sigma Aldrich, F6627), recombinant human IL-6 (Peprotech, 200-06), recombinant mouse IL-6 (Peprotech, 216-16) or human IFNA2 (Thermo Fisher, PHC4014). Following treatment, methyl thiazol tetrazolium (MTT, Sigma Aldrich) was added to the cultures to a final concentration of 5 mg ml^{-1} and incubated with the cells for a maximum of 4 h. MTT crystals were dissolved in DMSO and measured at 570 nm using a Multiskan GO scanner (Thermo Fisher Scientific). The percentage of viable cells was normalized to the measured absorbance of DMSO-treated cells. Each MTT experiment included three technical replicates, for which the average value represents the value of a single biological replicate.

Long-term clonogenic assays

BT549, MDA-MB-231 and 4T1 cells, wild-type cells, or with indicated genetic modification, were seeded into 6-well plates at a density of 2,000 cells per well and cultured with medium containing isotype IgG (Sanquin) or tocilizumab for at least 7 days. Medium was changed twice per week. Cells were fixed with 4% formaldehyde in PBS and stained with 0.1% crystal violet diluted in water. Growth was quantified by dissolving the crystal violet in 10% acetic acid, after which absorbance at 590 nm was measured for each well.

cGAMP ELISA

Cells were seeded in 10-cm culture dishes and treated as indicated for individual experiments. At 16 h before collection, medium was replaced with serum-free phenol red-free medium. To quantify extracellular cGAMP, medium were collected and centrifuged at ≥600*g* at 4 °C for 15 min. The supernatant was used for the ELISA assay. For intracellular cGAMP, the pellet of collected cells was lysed using LP2 lysis buffer (20 mM Tris HCl pH 7.7, 100 mM NaCl, 10 mM NaF, 20 mmol l^{-1} β-glycerophosphate, 5 mM $MgCl_2$, 0.1% (v/v) Triton X-100 and 5% (v/v) glycerol) and centrifuged at 10,000*g* for 15 min. Supernatant from this centrifuge step was used for a cGAMP ELISA. The cGAMP ELISA was performed using a cGAMP ELISA kit (Arbo Assay, K067-H1W) per the manufacturer's protocol.

RT–qPCR

For qPCR with reverse transcription (RT–qPCR), cell pellets were collected and immediately stored at −20 °C. RNA was isolated using a RNAeasy plus mini kit (Qiagen). cDNA was synthesized using M-MuLV reverse transcriptase (NEB) in the presence of a RNAse inhibitor (NEB) and a random primer mix (NEB) according to the manufacturer's protocol. RT–qPCR was performed using technical triplicates and biological replicates as indicated in the figure legends using iTaq Universal SYBR Green Supermix (Bio-Rad) on a LightCycler 480 Instrument (Roche). Tubulin or actin was used as the reference gene. Supplementary Table 1 lists the primers used.

Immunofluorescence staining and microscopy

For immunofluorescence experiments, cells were treated as described above and fixed in 4% formaldehyde for 15 min at room temperature. Next, cells were permeabilized with 0.1% Triton-X in PBS for 1 min and blocked with 3% FBS in PBS for 30 min at room temperature. Slides were incubated with a primary cGAS (1:250) or STING (1:250) antibody solution (3% FBS in PBS) for 1 h at room temperature. Following two washing steps, slides were incubated with a secondary Alexa 555 goat-anti-rabbit IgG (H+L) solution (3% FBS in PBS) for 30 min at room temperature protected from light. Slides were mounted with Vectashield mounting medium containing DAPI (Vectashield, H-1200) and were imaged using a TCS SP8 confocal microscope with a HC PL APO CS2 ×63/1.4 oil objective (Leica). Images were processed using ImageJ software (Fiji). A list of antibodies is provided in Supplementary Table 2.

Live cell imaging

For time-lapse imaging, 50,000 BT549, 4T1, MCF10A, MDA-MB-231, MDA-MB-436, E0771, HCC827, NCI-H1975, H292, OVMANA, RMG-I, JHOC5, SKOV3, OVCAR3, A2780, MeWo, A375 and SKMEL28 cells (with or without genetic modifications) were transduced with histone H2B–mCherry and seeded in a four-section imaging chamber (Greiner Bio-one, 627870) overnight before imaging. For reversine and AZD1775 treatment, 250 nM reversine or 500 nM AZD1775, respectively, was added 1 h before imaging started. For the quantification of kinetochores in micronuclei, BT549 cells expressing histone H2B–GFP–T2A–CENPB–mCherry were seeded on a four-section imaging chamber and treated with 250 nM reversine or 500 nM AZD1775 24 h before imaging. Cells were followed for at least 16 h on a DeltaVision Elite microscope (GE Healthcare), equipped with a CoolSNAP HQ2 camera, a ×20 0.75 NA or ×40 0.6 NA immersion objective (Olympus) and DeltaVision softWoRx software. Images were acquired at 7-min intervals and included *z*-stacks of 20 images at 0.4-µm intervals. Image analysis was done using ICY software (Institut Pasteur). All cells that entered mitosis and stayed in frame throughout the imaging session were included for analysis.

Quantification of apoptotic cells

To quantify apoptosis, BT549 and 4T1 cells were treated as indicated and collected. Cells were then stained with 5 µl of FITC-conjugated Annexin V antibody and propidium iodide (BioLegend, 640914) for 15 min. Next, cells were washed, resuspended in FACS buffer (3% FBS in PBS) and analysed on a Canto flow cytometer (BD Bioscience) using BD FACS Diva software (BD Bioscience). Data were analysed using FlowJo software (Treestar). The flow cytometry gating strategy is presented in Supplementary Fig. 2.

DNA fibre assays

To quantify replication speed, BT549 cells were pretreated with DMSO, 250 nM reversine or 500 nM AZD1775 and pulse-labelled with CldU (25 µM) for 20 min. Next, cells were washed with warm medium and pulse-labelled with IdU (250 µM) for 20 min. Cells were collected using trypsin and lysed on a microscope slide using lysis solution (0.5% SDS, 200 mM Tris (pH 7.4) and 50 mM EDTA). DNA fibres were spread by tilting the microscope slide, then air-dried and fixed in methanol and acetic acid (3:1) for 10 min. Next, DNA spreads were immersed in 2.5 M HCl for 75 min. Slides were blocked in blocking solution (5% BSA in PBS) for 30 min and incubated with primary antibodies for 60 min at room temperature. CldU was detected with rat anti-BrdU and IdU was detected with mouse anti-BrdU. Secondary antibodies used were Alexa 488-conjugated goat-anti-rat IgG and Alexa 647-conjugated goat-anti-mouse IgG. Images were acquired on a DeltaVision microscope with a ×60 1.41 NA objective. The fibre length of incorporated IdU was quantified using ImageJ. Antibody details are indicated in Supplementary Table 2.

Subcutaneous transplantation of tumour cells

For allografting of 4T1 tumours, 4T1 cells expressing either KIF2C or dnMCAK were collected, washed and diluted to 2.5×10^5 cells ml^{-1} in RPMI medium. Female Balb/c-OlaHsd or athymic nude-*Foxn1* (immune-proficient or immunocompromised, respectively) were subcutaneously injected with 5×10^4 cells with the indicated genotype per flank under anaesthesia of continuous inhalation of 2%

isoflurane gas. Mice (7-week-old female Balb/c-OlaHsd or athymic nude-*Foxn1*) were purchased from Envigo, where NOD:SCID (NOD.Cg-Prkdc<scid>Il2rg<tm1Wjl>/SzJ) mice were purchased from Charles River. The number of mice used for each experiment was determined using power calculation. For allografting of MDA-MB-231 or HCC827 tumour cells, MDA-MB-231 or HCC827 cells expressing either KIF2C or dnMCAK were collected, washed and diluted to indicated cell concentrations in RPMI medium. Female NOD:SCID mice (7 weeks old) were subcutaneously injected with 2.5×10^6 (MDA-MB-231) or 4×10^6 (HCC827) cells with the indicated genotype per flank under anaesthesia of continuous inhalation of 2% isoflurane gas. Before injection, cell suspensions were mixed 1:1 with Matrigel (Corning, 356234). All mice were monitored for tumour formation, and tumour length (L) and width (W) were measured twice per week using callipers. When tumours reached a volume of 100 mm^3, the frequency of measurements was increased to every 2 days. The tumour volume (V) was calculated as $V = (L \times W^2)/2$.

For the tocilizumab intervention experiments, interventions started when tumours reached a volume of 100 mm^3. Mice were randomized and received treatment twice per week with either isotype IgG control or tocilizumab (100 µg) by intraperitoneal injection. Mice were euthanized at the following humane end points: a total tumour volume exceeding 1.6 cm^3, tumour ulceration, necrotic tissue or a weight loss greater than 10% of the initial weight.

Mice were housed under specific pathogen-free conditions, maintained on a 12-h light–dark cycle and given water and food ad libitum in the animal facility in accordance with animal care regulations. All mice were closely monitored by the researchers, animal technicians and an independent veterinarian when necessary. All the procedures for the animal experiments were reviewed and approved by the Dutch Central Committee for animal testing (CCD) and the local Animal Welfare Committee (IvD) at the Central Animal Facility of the University Medical Centrum Groningen.

Immunohistochemistry

Slides (3 µm) of formalin-fixed and paraffin-embedded tissue were deparaffinized in xylene and rehydrated in decreasing ethanol solutions. Antigen retrieval was achieved by microwave heating for 15 min in 1 mM EDTA buffer pH 8. Endogenous peroxidase was blocked by incubating in 0.3% H_2O_2 in PBS solution for 30 min. After 1 h incubation with 1:100 diluted STING antibody or 1:200 diluted p-STAT1 antibody in PBS and 1%BSA, a secondary goat-anti-rabbit-HRP (1:100 in PBS, 1% BSA and 1% serum) was incubated for 30 min, followed by a rabbit-anti-goat-HRP (1:100 in PBS, 1% BSA and 1% serum) incubation for 30 min. After each step, slides were rinsed in PBS. Staining was visualized using 3,3′-diaminobenzidine tetrahydrochloride substrate (Sigma) for 10 min, followed by counterstaining with haematoxylin for 2 min and covered with mounting medium.

Immunohistochemistry images were scanned using a NanoZoomer S60 Digital slide scanner (Hamamatsu) and analysed with ImageScope (Aperio Technologies). Quantification of the stained slides was performed using the QuPath plug-in (ImageJ).

Derivation of primary T-ALL cultures and treatment

To derive primary T-ALL cultures, *Msh2*$^{-/-}$ mice, *Mad2*$^{fl/fl}$;*Trp53*$^{fl/fl}$;*Lck-cre* mice and *Mps1*$^{fl/fl}$;*Trp53*$^{fl/fl}$;*Lck-cre* mice were followed for signs of lymphoma (dyspnoea and weight loss) and euthanized when ill. The thymus was dissected (typically 1–2 g in size for the T-ALL samples) and homogenized through a 70-µm strainer to produce T-ALL suspensions. Primary suspension cultures of T-ALL were maintained under hypoxic conditions (37 °C, 5% CO_2, 3% O_2) and grown in RPMI 1640 medium, GlutaMAX supplement, HEPES (Gibco) supplemented with 10% FBS (Gibco), 1% P/S (Gibco), 1% nonessential amino acids (MEM-NEAA, Gibco) and 55 µM 2-mercaptoethanol (Sigma).

To test the effect of tocilizumab on the primary T-ALL cultures, cells with the indicated genotypes were seeded in equal numbers into 12-well plates (Greiner bio-one) and incubated for 96 h with either tocilizumab (Roche) or isotype IgG (Sanquin) added to the cell culture medium. After 96 h, cells were counted using a counting chamber (Bürker-Türk). Cell viability was assessed during counting by mixing cells in a 1:1 ratio with Trypan blue (Gibco).

Single-cell sequencing

To quantify aneuploidy and intratumour karyotype heterogeneity, primary T-ALL cells or passage 1–2 of primary cultured cells were collected, placed into lysis buffer and single-nuclei sorted using flow cytometry as previously described[39]. All samples (except for T302) were sequenced at about 0.01× coverage on a NextSeq 500 sequencer (Illumina). T302 was sequenced on a HiSeq 2500 sequencer (Illumina).

Sequencing reads were aligned to the mouse genome GRCm38 and analysed using the R package AneuFinder (v.1.14.0, R v.3.6.3)[38]. Copy number calling was performed using both dnacopy and edivisive algorithms, using a bin size of 1 Mb and a step size of 500 kb. To pass curation, libraries required 95% concordance between the two algorithms. Manual curation was then performed to remove libraries with low read counts (fewer than 10 reads per bin per copy). Heatmaps were plotted for all curated libraries using the edivisive results.

RNA sequencing

RNA was isolated using a RNeasy mini kit (Qiagen). RNA quality was examined using an Agilent 2100 Bioanalyzer (Agilent Technologies). Total RNA (250–500 ng) was used as input for mRNA enrichment using NEXTflex poly(A) beads (Bio Scientific) followed by library preparation using a NEXTflex Rapid Directional qRNA-Seq kit (Bio Scientific). Libraries were pooled, and paired-end sequencing was performed using a NextSeq 500 sequencer (Illumina). The sequencing reads were demultiplexed using sample-specific barcodes and changed into fastq files using bcl2fastq (Illumina; v.1.8.4).

Mate 1 contained the first stochastic labelling (STL) barcode, followed by the first bases of the sequenced fragments (cDNA), and mate 2 only contained the second STL barcode (length of mate 1: 74 bases; length of mate 2: 9 bases; STL barcode sequences have a length of 8 bases).

The quality of the data was assessed using FastQC (v.0.11.8)[48]. The STL barcodes were separated from the sequenced fragments using an in-house Perl script. Low-quality bases and parts of adapter sequences were removed from the remaining fragment sequence of mate 1 with Cutadapt (v.1.12; settings: $q = 15$, $O = 5$, $e = 0.1$, $m = 36$)[49]. Sequenced polyA tails were also removed using a polyT sequence as adapter sequences (-g "T{100}"; reverse complement after sequencing; trimmed at the beginning). Reads shorter than 36 bases were discarded.

The trimmed reads (sequenced fragments; cDNA) were subsequently aligned to all known human cDNA sequences (GRCh38, Ensembl release 101, including ncrna genes) using HISAT2 (v.2.1.0; settings: $k = 1000$, --norc)[50] . The number of reported alignments, k, was given a high number to not miss any alignment results. Reads were only mapped to the forward strand (directional sequencing). Reads that mapped to multiple genes were removed (unknown origin). Duplicates were detected by comparing the transcript identity (ID), position and barcode sequence combinations. A read is considered duplicate when this combination already exists. Corresponding gene IDs were used to get the total read count for each gene. The link between transcript and gene ID was obtained from the description lines of the cDNA sequences (fasta files). The abovementioned steps were performed using in-house Perl scripts (Perl v.5.28.1).

Differential expression was computed using DESeq2 (ref. [51]), and significance was tested with a default Wald test between two biological replicates each of reversine-treated and DMSO-treated samples. Gene IDs were mapped to gene symbols using Ensembl 104 (ref. [52]). Functional annotations were provided using the MSigDB Hallmark collection[53] and discriminant regulon enrichment analysis (DoRothEA[54]) transcription factor–target annotations of gene sets. Fold changes of

gene sets were computed as the average change of gene set members versus non-members, and their significance determined by a linear model testing for a difference in the DESeq2 Wald statistic between gene set members and non-members. Fold-changes in *cGAS*^{KO} cells shown in Fig. 1g were corrected for wild-type contamination.

TCGA analysis

Read counts of the TCGA breast cancer (BRCA), lung cancer (LUAD and LUSC), ovarian cancer (OV) and melanoma (SKCM) cohorts were downloaded using the R (v.4.0.5) package TCGAbiolinks (v.2.18.0)[55] and variance-stabilizing transformed with DESeq2 (v.1.31.3)[51]. Gene IDs were mapped to gene symbols using Ensembl 104 (ref. [52]). Gene sets were scored using gene set variation analysis (GSVA R package[56], v.1.38.2) using the MSigDB Hallmark collection[53] for IFN and IL-6–STAT3 signalling, and the CIN70 gene set[32] as a measure of chromosomal instability. Aneuploidy was scored as the mean deviation of DNA copy number from the sample average according to SNP6 copy number estimation. Purity estimates were obtained from ESTIMATE algorithm[57]. Oestrogen receptor and progesterone receptor (ER/PR) status, HER2 status and overall survival status/times were assigned as per TCGA metadata.

Associations between the expression of two genes, or a gene with a gene set, were computed using a linear regression model with either the value obtained for a sample (referred to as 'sample') or by regressing out the non-tumour contribution (referred to as 'cancer'). For the latter, (1) a linear model between the response variable and tumour purity as defined by ESTIMATE was fitted, and (2) the difference between the expected expression value of a theoretically pure sample (extrapolating ESTIMATE purity to (1) and the expected expression of the mixed sample (at an ESTIMATE purity of the actual sample) was subtracted, and (3) a linear model on the new response variables was calculated. This approach was chosen over adding a covariate in the regression because it allows for visualization of the corrected values.

For breast cancer survival associations, the cohort was split by the sample-level IFN response score and purity-corrected IL-6 signalling score (MSigDB Hallmarks, as indicated on Fig. 3g), as well as their aneuploidy (dichotomized above and below 20% of the genome having a copy number of one gain or loss) and CIN70 score (dichotomized at the bimodal density minimum of the GSVA score at 0, as in Extended Data Fig. 9a). For CIN70^{high} and CIN70^{low} separately, a multivariate Cox regression was performed with the age at diagnosis and tumour purity as covariates, and their immune class as main factor of interest (R package survival, v.3.2). In addition, another Cox regression included the 'E2F targets' gene set expression as a covariate for cell proliferation correction[58]. *P* values reported represent the IL-6-driven partition over the reference (IFN^{high}). Additional survival associations in TCGA LUSC/LUAD, OV and SKCM used the continuous cancer-specific IL-6–STAT3 gene set score directly (correcting for patient age and sample purity; LUSC/LUAD), or the difference between IL-6–STAT3 and IFN response (OV, SKCM). Gene expression *z*-scores for CGAS, IL-6 and IL-6R were obtained from a variance stabilizing transformation (DESeq2) on the gene-level read counts.

DepMap analysis

For a large set of cancer cell lines, gene-level essentiality scores (CRISPR knockout-based), copy number and mRNA expression data were obtained from DepMap release 21Q2, using the Broad Institute's DepMap portal[33,48]. Cell lines with fibroblast, teratoma, unknown, engineered or of non-cancerous origin were excluded from analysis. A linear model was fitted to identify associations between *IL6R* mRNA expression and gene essentiality scores using R 4.0.0. For REACTOME gene sets[59] (obtained from MSigDB, v.7.4), Student's *t*-tests were performed between the false discovery rate (FDR) values of genes in the gene set versus FDR values of genes not in the gene set. The gene set dependency score was computed by multiplying the resulting FDR value per gene set with the sign of the *t*-statistic. To control false detection rate, *P* values were corrected using the Benjamini–Hochberg method.

Statistics and reproducibility

The group sizes, number of replicates and explanations of mean and error bars are provided in the figure legends. Statistical tests were performed using GraphPad Prism 9.0 (GraphPad Software). For comparisons between two experimental groups, unpaired two-tailed *t*-tests were used, unless stated otherwise. Survival curves were analysed using log-rank (Mantel–Cox) test. Data are shown as the mean ± s.e.m. unless specified otherwise. $*P < 0.05$, $**P < 0.01$, $***P < 0.005$, and exact *P* values are stated in the source data for each figure panel. Each representative image (Extended Data Figs. 1j, 2a,e, 3a,j, 5c,d, 6a,b,d,g and 8p) is from a dataset composed of at least two independent experiments.

Reporting summary

Further information on research design is available in the Nature Research Reporting Summary linked to this paper.

Data availability

All data from this study are available by request by contacting F.F. The RNA sequencing data have been deposited into ArrayExpress under the accession number E-MTAB-10923. Shallow single-cell whole-genome sequencing data have been deposited into the European Nucleotide Archive under the accession number PRJEB49800. Source data are provided with this paper.

Code availability

Analysis code is available at https://github.com/mschubert/cgas_ko.

46. Ran, F. A. et al. Genome engineering using the CRISPR–Cas9 system. *Nat. Protoc.* **8**, 2281–2308 (2013).
47. Schukken, K. The consequences of aneuploidy and chromosome instability: survival, cell death and cancer. PhD thesis, Univ. Groningen (2020).
48. FastQC: a quality control tool for high throughput sequence data version 0.11.9 (Babraham Bioinformatics, 2019).
49. Martin, M. Cutadapt removes adapter sequences from high-throughput sequencing reads. *EMBnet J.* **17**, 10–12 (2011).
50. Kim, D., Langmead, B. & Salzberg, S. L. HISAT: a fast spliced aligner with low memory requirements. *Nat. Methods* **12**, 357–360 (2015).
51. Love, M. I., Huber, W. & Anders, S. Moderated estimation of fold change and dispersion for RNA-seq data with DESeq2. *Genome Biol.* **15**, 550 (2014).
52. Howe, K. L. et al. Ensembl 2021. *Nucleic Acids Res.* **49**, D884–D891 (2021).
53. Liberzon, A. et al. The Molecular Signatures Database Hallmark Gene Set Collection. *Cell Syst.* **1**, 417–425 (2015).
54. Garcia-Alonso, L. et al. Transcription factor activities enhance markers of drug sensitivity in cancer. *Cancer Res.* **78**, 769–780 (2018).
55. Colaprico, A. et al. TCGAbiolinks: an R/Bioconductor package for integrative analysis of TCGA data. *Nucleic Acids Res.* **44**, e71 (2016).
56. Hänzelmann, S., Castelo, R. & Guinney, J. GSVA: gene set variation analysis for microarray and RNA-seq data. *BMC Bioinformatics* **14**, 7 (2013).
57. Yoshihara, K. et al. Inferring tumour purity and stromal and immune cell admixture from expression data. *Nat. Commun.* **4**, 2612 (2013).
58. Buccitelli, C. et al. Pan-cancer analysis distinguishes transcriptional changes of aneuploidy from proliferation. *Genome Res.* **27**, 501–511 (2017).
59. Jassal, B. et al. The reactome pathway knowledgebase. *Nucleic Acids Res.* **48**, D498–D503 (2020).

Acknowledgements We are grateful to the members of the Bruggeman, de Bruyn, van Vugt and Foijer laboratories for fruitful discussions. We thank M. Weij and D. Eichorn at the central animal facility for assistance with animal experiments; J. Teunis at the flow cytometry facility for help with flow cytometry; R. Arjaans and N. Halsema at the UMCG/ERIBA Research Sequencing facility for help with RNA sequencing library preparation and (single cell) sequencing; and M. Broekhuis and J. Seiler at the UMCG/ERIBA iPSC/CRISPR facility for advice regarding the CRISPR knockout experiments. This work was supported by Dutch Cancer Society grants to F.F. (2015-RUG-7833 & 2018-RUG-11457) and M.A.T.M.v.V. (2018-RUG-11352), UMCG research fellowships to C.H. and M. Requesens, and a UMCG Cancer Research Fund (KRF) grant to C.H.

Author contributions C.H., M.d.B., M.A.T.M.v.V. and F.F. conceived the project. C.H. and F.F. designed all the experiments. C.H., A.E.T., A.v.d.B., L.A.R., P.L.B. and T.v.d.S. performed the in vitro experiments. C.H., A.E.T. and M. Requesens performed the animal experiments. M.S., M. Roorda, M.C. and R.W. performed data analyses. W.P. contributed reagents. D.C.J.S. oversaw RNA and single-cell sequencing. B.v.d.V. oversaw histological staining. C.H. and F.F. wrote the

manuscript with input from M.S., M.d.B. and M.A.T.M.v.V. All authors reviewed and approved the manuscript.

Competing interests M.A.T.M.v.V. has acted on the Scientific Advisory Board of Repare Therapeutics, which is unrelated to this work. B.v.d.V has acted as a consultant or scientific advisory board member (on request) for Visiopharm, Philips, MSD/Merck and as a speaker for Visiopharm, Diaceutics and MSD/Merck for which UMCG was compensated. This is all unrelated to this work. The other authors declare no competing interests.

Additional information

Supplementary information The online version contains supplementary material available at https://doi.org/10.1038/s41586-022-04847-2.

Correspondence and requests for materials should be addressed to Marco de Bruyn, Marcel A. T. M. van Vugt or Floris Foijer.

Peer review information *Nature* thanks Glen Barber and the other, anonymous, reviewer(s) for their contribution to the peer review of this work. Peer reviewer reports are available.

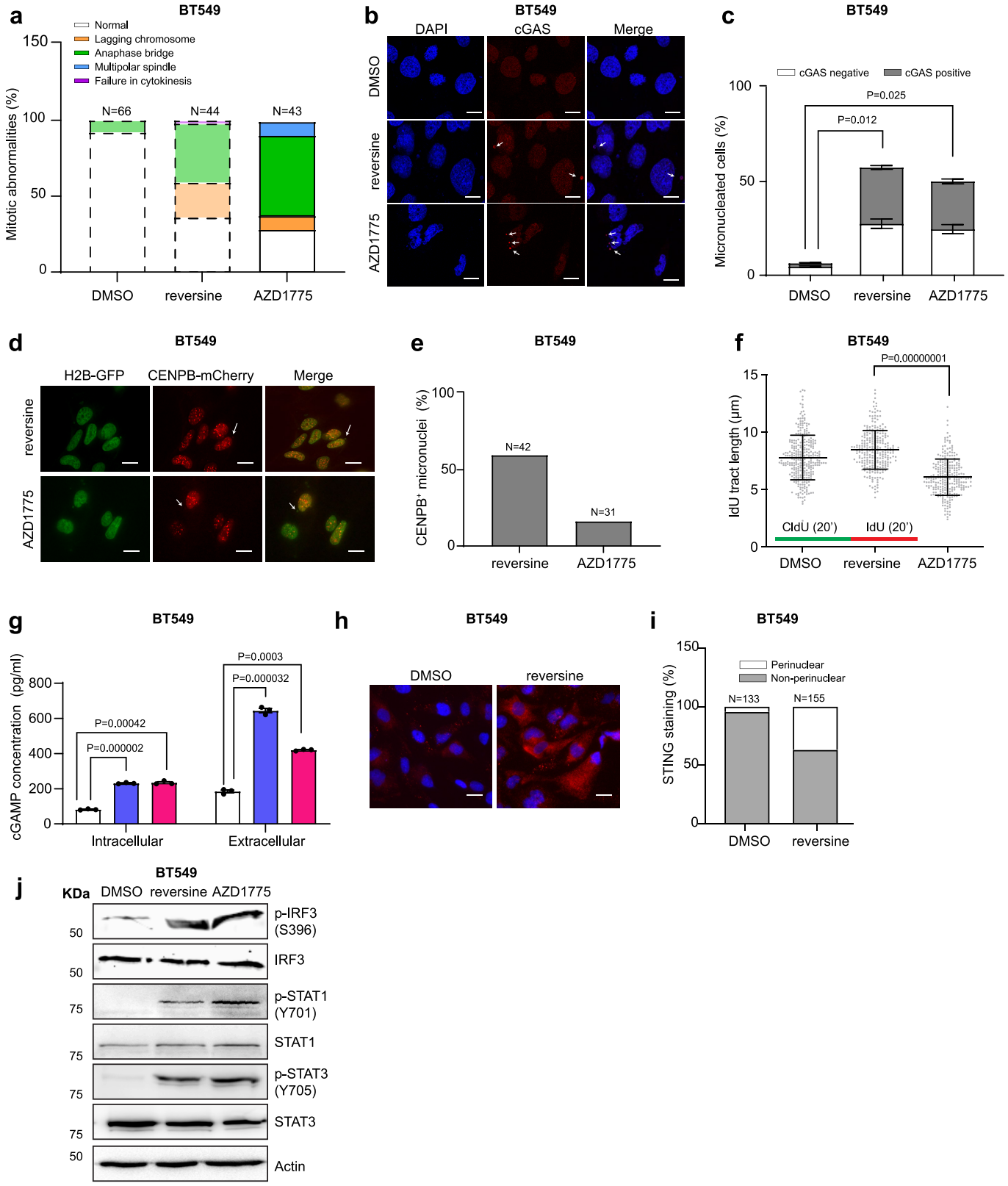

Extended Data Fig. 1 | See next page for caption.

Extended Data Fig. 1 | Inhibition of Mps1 and Wee1 lead to activation of cGAS signalling in BT549 TNBC cells. a) Quantification of mitotic abnormalities observed in BT549 cells expressing Histone H2B-mCherry treated with DMSO, 250 nM reversine or 500 nM AZD1775 assessed by live cell imaging, the number of assessed mitotic cells – n - is indicated in the figure. Dashed lines indicate that these measurements (DMSO and reversine-treated) cells are also shown in Fig. 1b. **b)** Representative immunofluorescence images of DMSO-, 250 nM reversine-, or 500 nM AZD1775-treated BT549 cells stained with DAPI (DNA) and an anti-cGAS antibody, scale bar equals to 10 µm. Arrows point at cGAS positive micronuclei. **c)** Quantification of cGAS positive micronuclei in DMSO-, 250 nM reversine, or 500 nM AZD1775-treated BT549 cells. Error bars represent the s.e.m, significance was tested with a two-sided t-test. **d)** Representative images of 250 nM reversine- or 500 nM AZD1775-treated BT549 cells expressing Histone H2B-GFP and CENPB-mCherry, scale bar equals to 5 µm. Arrow indicates CENPB positive micronuclei. **e)** Quantification of CENPB positive micronuclei observed in 250 nM reversine- or 500 nM AZD1775-treated BT549 cells, the number of quantified cells – n – is indicated in the figure. **f)** DNA fibre assay showing decreased fibre size for AZD1775-, but not reversine-treated cells indicating replication stress in the former. BT549 cells were treated with DMSO, 250 nM reversine, or 500 nM AZD1775. For each condition, 260 fibres from 2 experiments were analysed and individual IdU track lengths are displayed together with the mean and standard deviation value. **g)** cGAMP levels quantified in cell lysates (intracellular) or in harvested culture media (extracellular) from wild type BT549 cells incubated with DMSO, 250 nM reversine, or 500 nM AZD1775 for 48 hours. cGAMP levels were normalised to harvested cell numbers. **h)** Representative images of 250 nM reversine- or DMSO-treated BT549 cells stained with DAPI (DNA) and an anti-STING antibody showing peri-nuclear STING localization following reversine treatment. Scale bar equals to 5 µm. **i)** Quantification of cells with perinuclear or non-perinuclear STING localization as shown in (**h**). The number of quantified cells – n – is indicated in the figure. **j)** Immunoblots on lysates from 48 hours DMSO, 250 nM reversine or 500 nM AZD1775-treated BT549 cells showing phosphorylated and total IRF3, STAT1 and STAT3. β-Actin is shown as a loading control. Error bars in (**c**, **g**) represent s.e.m, n=3 biological replicates (**c**, **g**), significance was tested with a two-sided t-test.

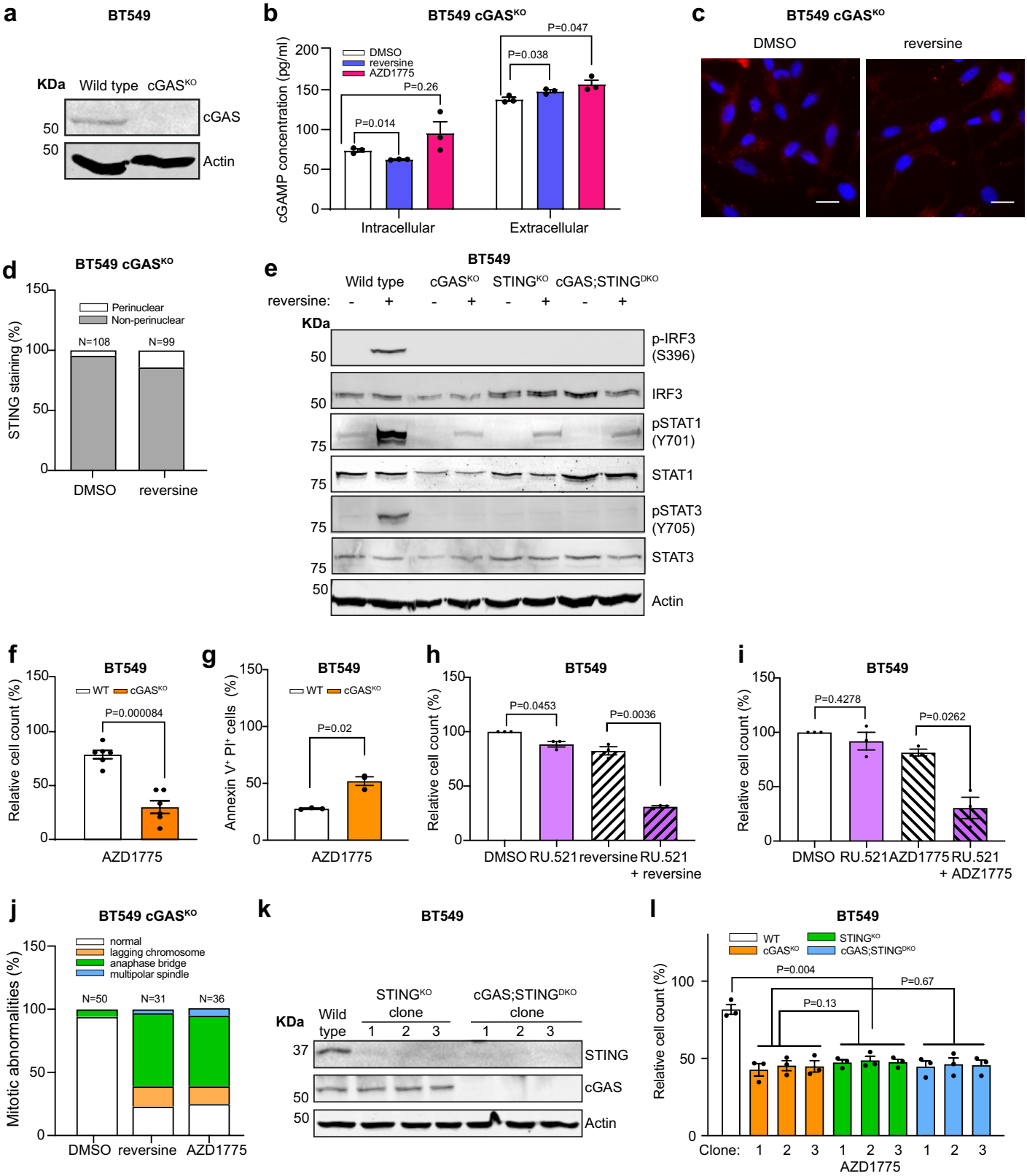

Extended Data Fig. 2 | See next page for caption.

Extended Data Fig. 2 | Loss of cGAS or STING in BT549 TNBC cells results in increased sensitivity to Mps1 or Wee1 inhibition. a) Immunoblots of wild type and *cGAS*^{KO} BT549 cell lysates stained with anti-cGAS and anti-ß-actin antibodies. ß-Actin is used as a loading control. **b)** cGAMP levels quantified in cell lysates (intracellular) or in tissue culture media (extracellular) isolated from *cGAS*^{KO} BT549 cells incubated with DMSO, 250 nM reversine, or 500 nM AZD1775 for 48 hours. cGAMP levels were normalised to harvested cell numbers. **c)** Representative images of 250 nM reversine- or DMSO-treated BT549 *cGAS*^{KO} cells stained with DAPI (DNA) and an anti-STING antibody. Scale bar equals 5 µm. **d)** Quantification of cells with peri-nuclear or non-peri-nuclear STING localization. The number of quantified cells – n – is indicated in the figure. **e)** Immunoblots of cell lysates from wild type, *cGAS*^{KO}, *STING*^{KO}, and *cGAS; STING*^{DKO} BT549 cells treated with DMSO or 250 nM reversine stained with anti-p-IRF3 (Serine 396), anti-IRF3, anti-p-STAT1 (Tyrosine 701), anti-STAT1, anti-p-STAT3 (Tyrosine 705), anti-STAT3, or anti-ß-Actin. ß-Actin is used as a loading control. **f)** DMSO-normalised cell count of wild type or *cGAS*^{KO} BT549 cells treated with 500 nM AZD1775 for 48 hours. **g)** Percentage of apoptotic cells quantified by Annexin V staining of wild type or *cGAS*^{KO} BT549 cells treated with 500 nM AZD1775 for 48 hours. **h)** DMSO-normalised cell count of wild type BT549 cells treated with a combination of 2.5 µM RU.521 and 250 nM reversine for 72 hours. **i)** DMSO-normalised cell count of wild type BT549 cells treated with a combination of 2.5 µM RU.521 and 500 nM AZD1775 for 48 hours. **j)** Quantification of mitotic abnormalities observed in *cGAS*^{KO} BT549 cells expressing Histone H2B-mCherry treated with DMSO, 250 nM reversine or 500 nM AZD1775 assessed by live cell imaging, the number of assessed mitotic cells – n –is indicated in the figure. **k)** Immunoblots of wild type, *STING*^{KO}, or *cGAS; STING*^{DKO} BT549 cell lysates stained using anti-STING, anti-cGAS and anti-β Actin antibodies. ß-Actin is used as a loading control. **l)** Control DMSO-normalised cell counts of wild type, *cGAS*^{KO}, *STING*^{KO}, or *cGAS; STING*^{DKO} BT549 cells treated with 500 nM AZD1775 for 48 hours. Error bars in (**b**, **f**–**i**, **l**) represent the s.e.m, n=3 biological replicates (**b**, **g**–**i**, **l**), n=6 biological replicates (**f**), significance was tested with a two-sided t-test.

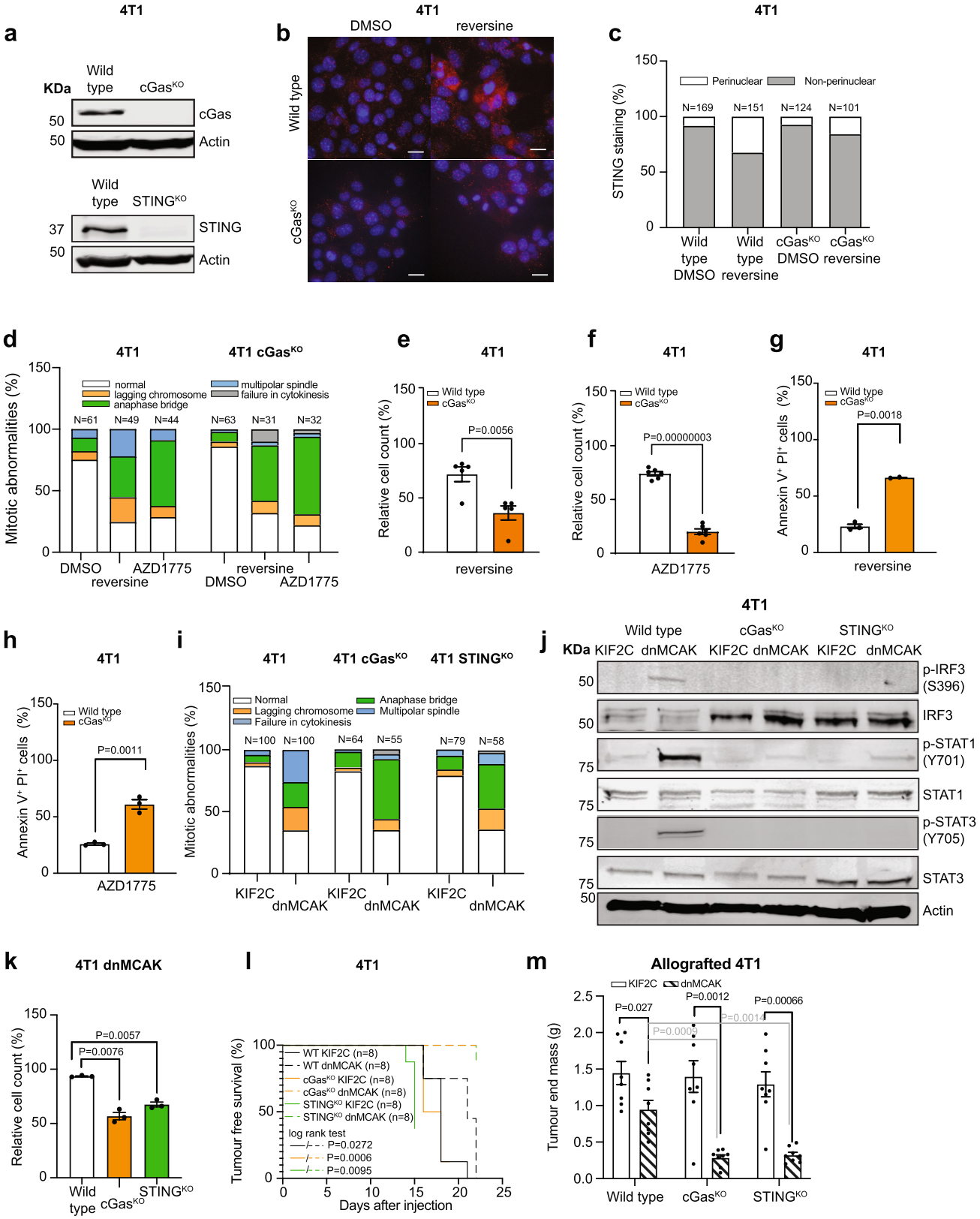

Extended Data Fig. 3 | See next page for caption.

Extended Data Fig. 3 | Loss of cGas signalling sensitizes mouse 4T1 TNBC cells to acute and chronic CIN in cell cultures and *in vivo*. a) Immunoblots of wild type, *cGas*^{KO} and *STING*^{KO} 4T1 cell lysates to validate loss of cGas (top panel) and STING (bottom panel) protein. ß-Actin is used as a loading control. **b)** Representative images of DMSO- or 250 nM reversine-treated wild type or *cGas*^{KO} 4T1 cells stained with DAPI (DNA) and anti-STING antibody showing reduced peri-nuclear STING localization in cGas^{KO} 4T1 cells. Scale bar equals to 5 µm. **c)** Quantification of cells with peri-nuclear and non-perinuclear localization of STING. The number of quantified cells – n – is shown in the figure. **d**) Quantification of mitotic abnormalities observed in wild type or *cGas*^{KO} 4T1 cells expressing Histone H2B-mCherry treated with DMSO, 250 nM reversine, or 500 nM AZD1775. **e**–**f)** Control DMSO-normalised cell counts for wild type or *cGas*^{KO} 4T1 cells treated with 250 nM reversine for 72 hours (**e**) or 500 nM AZD1775 for 48 hours (**f**). **g**–**h)** Fraction of apoptotic cells quantified by Annexin V staining of wild type or *cGas*^{KO} 4T1 cells treated with 250 nM reversine for 72 hours (**g**) or 500 nM AZD1775 for 48 hours (**h**). **i)** Quantification of mitotic abnormalities observed in wild type; *cGas*^{KO}, or *STING*^{KO} 4T1 cells expressing KIF2C (CIN^{low}) or dnMCAK (CIN^{high}). **j)** Immunoblots of lysates from wild type, cGas^{KO}, or *STING*^{KO} KIF2C (CIN^{low}) or dnMCAK (CIN^{high}) expressing 4T1 cells for phosphorylated and total IRF3, STAT1 and STAT3. ß-Actin is used as a loading control. **k)** KIF2C-normalised cell counts for wild type, *cGas*^{KO}, or *STING*^{KO} dnMCAK expressing 4T1 cells. **l)** Tumour-free survival of KIF2C (CIN^{low}) or dnMCAK (CIN^{high}) wild type, *cGas*^{KO}, or *STING*^{KO} cells transplanted to immunocompetent Balb/c and followed for up to 22 days. Tumours were included in the survival curve if they reached a volume of 500 mm^3 or larger. **m)** End mass of tumours harvested shown in Fig. 1f and Extended Data Fig. 3l. Error bars in (**e**–**h**, **k**–**m**) indicate the s.e.m, n=5 biological replicates (**e**), n= 6 biological replicates (**f**), n=3 biological replicates (**g**–**h**, **K**), n=8 biological replicates (**m**), significance was tested with a two-sided t-test.

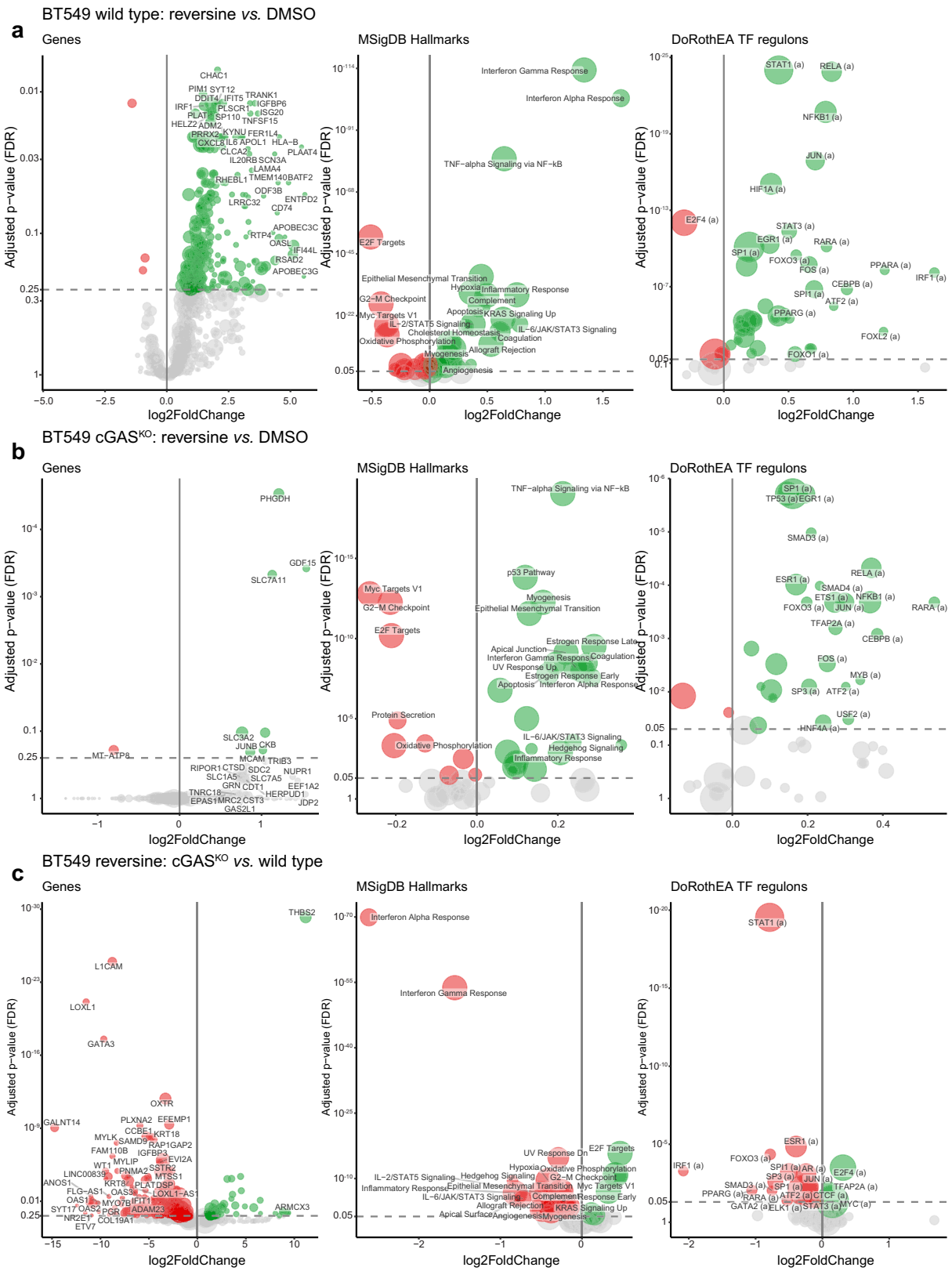

Extended Data Fig. 4 | Effect of cGAS on differential expression of reversine-treated BT549 cells. a) Differential expression of a parental BT549 cell line upon 48h of treatment with reversine vs. DMSO. X-axis shows log2 fold change, y-axis FDR-adjusted p-values. Size of the circle corresponds to the expression level in the untreated condition. Biological processes are characterised as MSigDB Hallmark (middle) and DoRothEA transcription factor target genes (right). Significance of gene sets was tested comparing the Wald statistic of genes within *vs.* genes outside the set using a linear model. Size of the circle corresponds to the number of genes in the set. **b)** Differential expression of *cGAS*^{KO} BT549 cells reversine *vs.* DMSO shows a clearly diminished transcriptional response, indicating that most of the transcriptional response to CIN is driven by cGAS, characterised by a drop of interferon response genes (middle) and STAT1/NF-kB-responsive genes. **c)** Differential expression of reversine-treated BT549 cells between *cGAS*^{KO} and wild type (parental) confirms a lower expression of interferon and STAT1-driven genes in the knockout *vs.* the wild type condition.

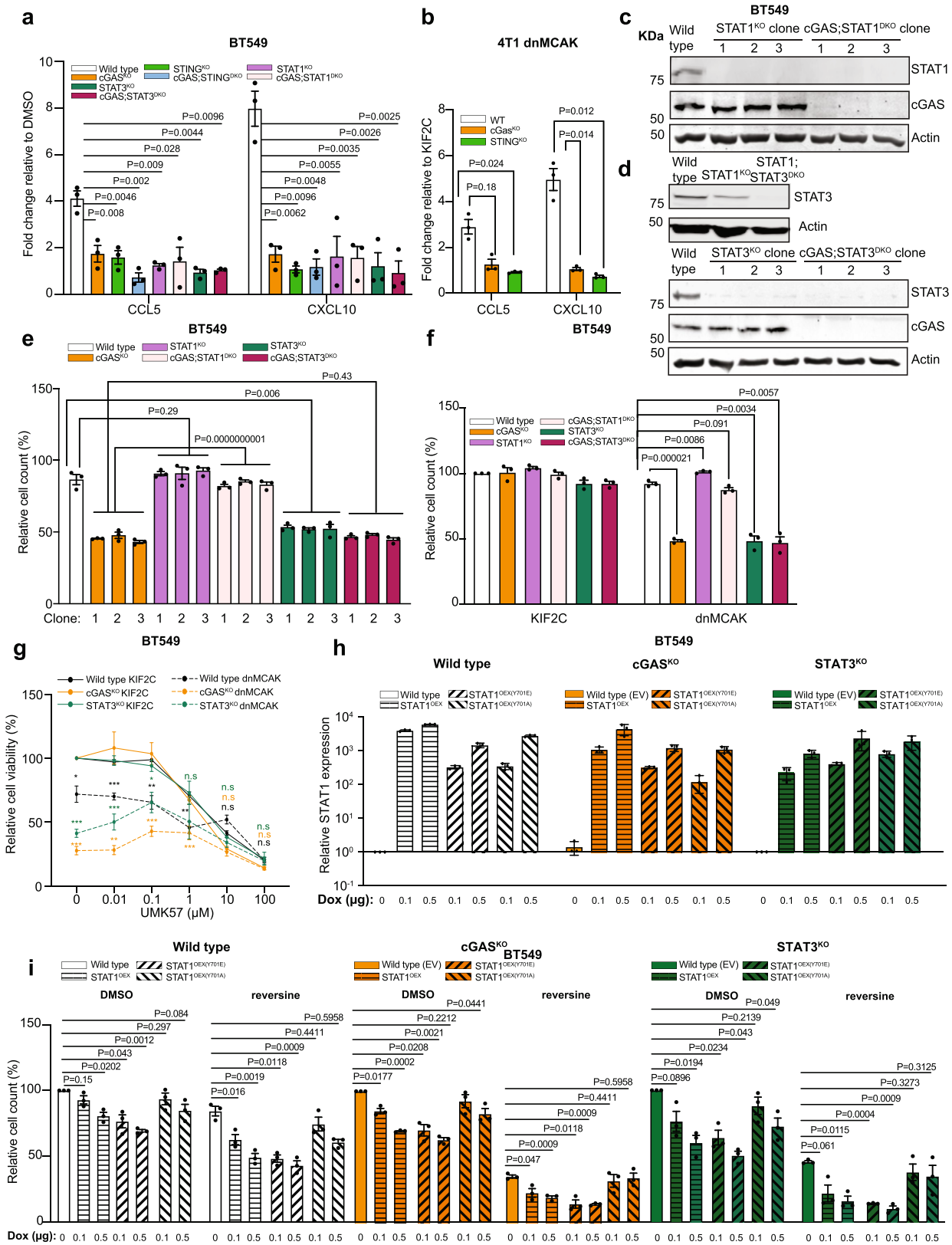

Extended Data Fig. 5 | See next page for caption.

Extended Data Fig. 5 | Acute and chronic CIN activate STAT1 and STAT3 signalling with STAT1 promoting and STAT3 preventing CIN-induced loss of viability in BT549 and 4T1 TNBC cells. a) Control DMSO-normalised CCL5 and CXCL10 expression in 250 nM reversine-treated wild type, *cGAS*^{KO}, *STING*^{KO}, *cGAS; STING*^{DKO}, *STAT1*^{KO}, *cGAS; STAT1*^{DKO}, *STAT3*^{KO}, or *cGAS; STAT3*^{DKO} BT549 cells determined by quantitative RT-PCR. **b)** Control KIF2C-normalised Ccl5 and Cxcl10 expression in dnMCAK expressing wild type, *cGas*^{KO}, and *STING*^{KO} 4T1 cells determined by quantitative RT-PCR. **c)** Immunoblots of wild type, *STAT1*^{KO}, or *cGAS; STAT1*^{DKO} BT549 cell lysates showing STAT1 or cGAS expression (top panels) and of wild type, *STAT1*^{KO} and *STAT1; STAT3*^{DKO} cell lysates showing STAT3 expression. ß-Actin is shown as a loading control. **d)** Immunoblots of wild type, *STAT3*^{KO}, or *cGAS; STAT3*^{DKO} BT549 cell lysates showing STAT1 or cGAS expression. ß-Actin is shown as a loading control. **e)** Control DMSO-normalised cell counts for wild type, *cGAS*^{KO}, *STAT1*^{KO}, *cGAS ;STAT1*^{DKO}, *STAT3*^{KO}, and *cGAS; STAT3*^{DKO} BT549 cells treated with 500 nM AZD1775 for 48 hours. **f)** Relative cell counts of doxycycline-inducible KIF2C- (CIN^{low}) or dnMCAK- (CIN^{high}) expressing wild type, *cGAS*^{KO}, *STAT1*^{KO}, *cGAS; STAT1*^{DKO}, *STAT3*^{KO} or *cGAS; STAT3*^{DKO} BT549 cells. **g)** DMSO-normalised cell viability of wildtype, *cGAS*^{KO} or STAT3^{KO} BT549 cells expressing KIF2C or dnMCAK across a range of UMK-57 concentrations. **h)** Relative expression of doxycycline-induced STAT1 (mutants) compared to endogenous STAT1 transcripts determined by quantitative RT PCR. Cells were treated with 100 ng/ml and 500 ng/m of doxycycline as indicated. **i)** DMSO-normalised cell counts of wild type, *cGAS*^{KO}, or *STAT3*^{KO} BT549 cells with overexpression of wild type STAT1, constitutive active STAT1^{Y701E}, or inactive STAT1^{Y701A}. Error bars in (**a**–**b**, **e**–**f**, **g**, **i**) represent the s.e.m, while those in (**h**) represent the standard deviation. n=3 biological replicates (**a**–**b**, **e**–**f**, **g**, **i**) or n=3 technical replicates (**h**). Significance was tested by two-sided t-test. Cells were treated for 48 hours (**a**) or 72 hours (**e**–**i**). * P<0.05, ** P<0.01, *** P<0.0005 (**g**), exact P-values are specified in Source Data Extended Data Fig. 5.

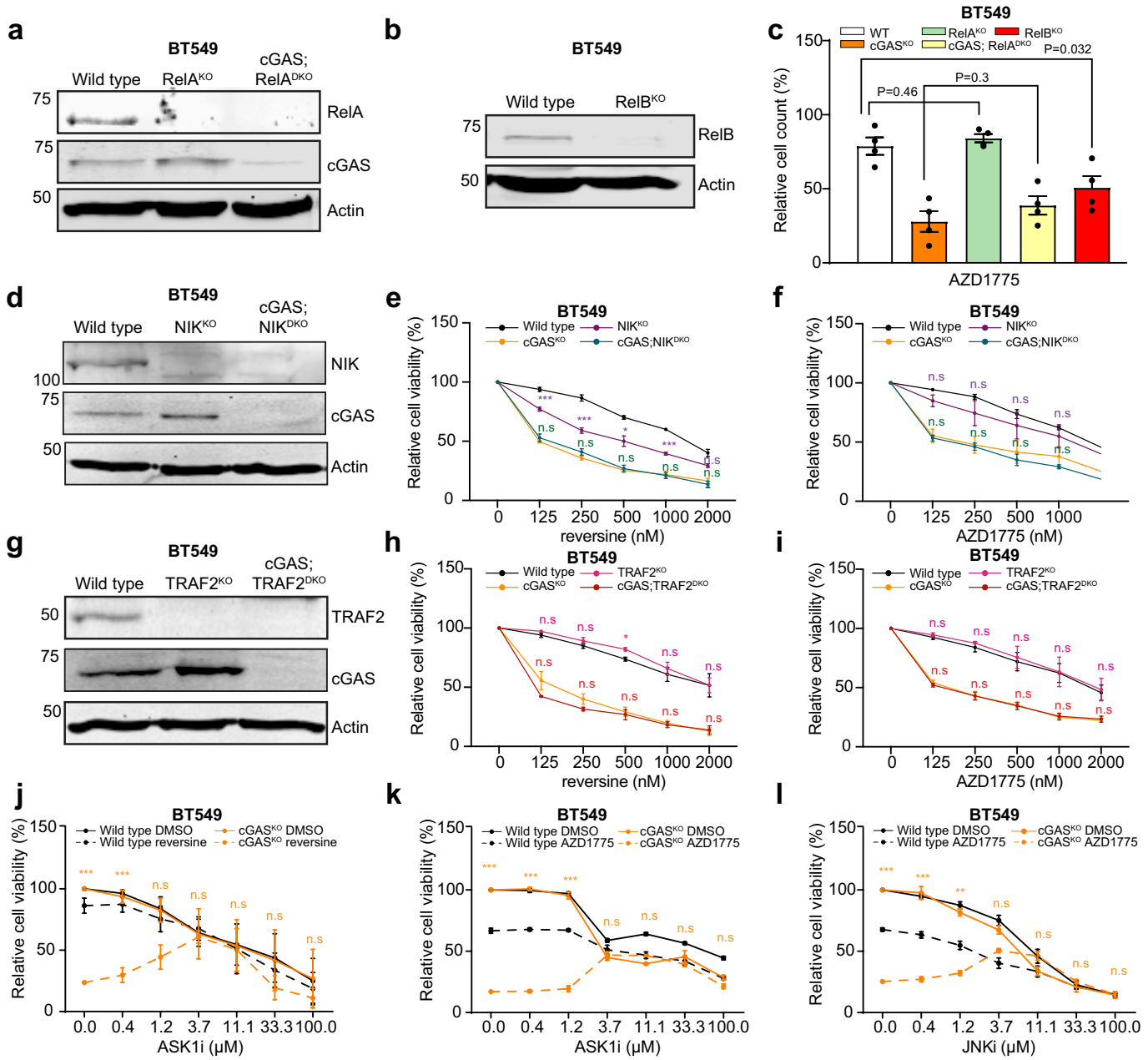

Extended Data Fig. 6 | BT549 cells rely on non-canonical NF-kB signalling, but not canonical NF-kB signalling for survival to prevent CIN-induced cell death. a) Immunoblots of wild type, *RelA*^{KO}, or *cGAS; RelA*^{DKO} BT549 cell lysates showing RelA and cGAS protein levels. ß-Actin is used as a loading control. **b)** Immunoblots of wild type, *RelB*^{KO}, or *cGAS; RelB*^{DKO} BT549 cell lysates showing RelB and cGAS protein levels. ß-Actin is used as a loading control. **c)** Control DMSO-normalised cell counts of wild type, *cGAS*^{KO}, *RelA*^{KO}, or *cGAS; RelA*^{DKO}, or *RelB*^{KO} BT549 cells treated with 500 nM AZD1775 for 48 hours. **d)** Immunoblots of wild type, *NIK*^{KO}, *cGAS; NIK*^{DKO} BT549 cell lysates showing NIK and cGAS protein levels. ß-Actin is used as a loading control. **e–f)** Control DMSO-normalised cell viability of wild type, *cGAS*^{KO}, *NIK*^{KO}, or *cGAS; NIK*^{DKO} for increasing reversine (**e**) or AZD1775 concentrations (**f**), treated for 72 or 48 hours, respectively. **g)** Immunoblots of wild type, *TRAF2*^{KO}, and *cGAS; TRAF2*^{DKO} BT549 cell lysates showing TRAF2 and cGAS protein levels. ß-Actin is used as a loading control. **h–i)** Control DMSO-normalised cell viability of wild type, *cGAS*^{KO}, *TRAF2*^{KO}, or *cGAS; TRAF2*^{DKO} for increasing reversine (**h**) or AZD1775 concentrations (**i**), treated for 72 or 48 hours, respectively. **j)** Control DMSO-normalised cell viability of DMSO- or 250 nM reversine-treated wild type or *cGAS*^{KO} BT549 cells across a range of ASK1 inhibitor concentrations. **k–l)** Control DMSO-normalised cell viability of DMSO- or 500 nM AZD1775-treated wild type or *cGAS*^{KO} BT549 cells across a range of (**k**) ASK1 inhibitor or (**l**) JNK inhibitor concentrations. Bars in (**c**, **e–f**, **h–i**) represent the s.e.m, n=4 biological replicates (**c**), n=3 biological replicates (**e–f**, **h–i**). Significance was tested with a two-sided t-test. *P<0.05, **P<0.01, ***P<0.005, exact P-values are specified in Source Data Extended Data Fig. 6.

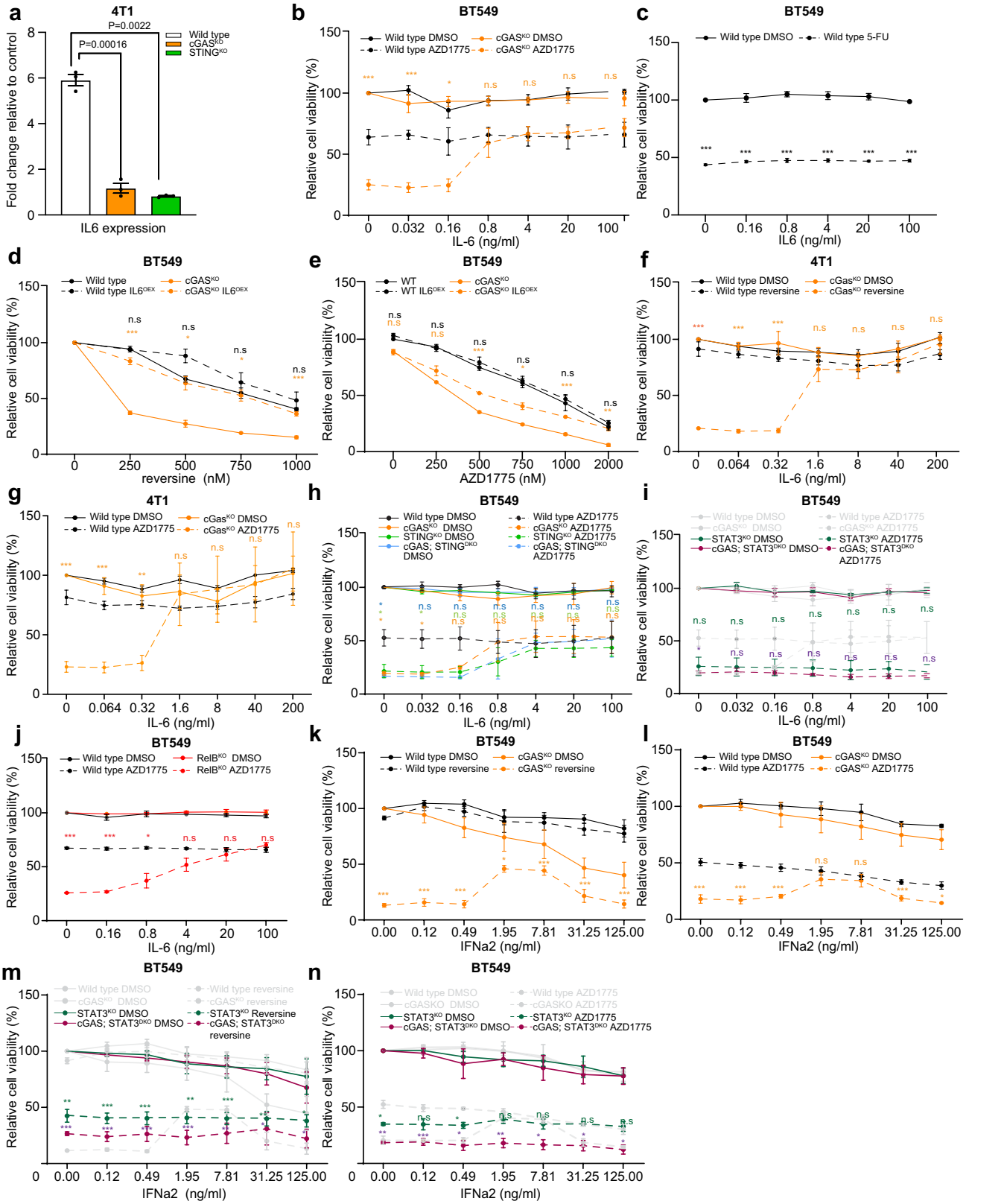

Extended Data Fig. 7 | See next page for caption.

Extended Data Fig. 7 | IL6 is induced in a cGAS-STING dependent manner following drug-induced CIN in TNBC cells to promote cell survival. **a)** Control KIF2C-normalised IL6 expression in dnMCAK expressing wildtype, *cGAS*^{KO} and *STING*^{KO} 4T1 cells determined by quantitative RT-PCR. **b)** Cell viability of DMSO- or 500 nM AZD1775-treated wild type or *cGAS*^{KO} BT549 cells supplemented with increasing quantities of IL6. **c)** Cell viability of DMSO- or 10 μM 5-fluoro-uracil (5-FU)-treated wild type BT549 cells supplemented with increasing quantities of IL6 to show that IL6 does not increase viability for a compound that does not provoke CIN. **d**–**e)** Control DMSO-normalised cell viability of wild type or *cGAS*^{KO} BT549 cells with or without overexpression of IL6 with increasing reversine (**d**) or AZD1775 concentrations (**e**). **f)** Control DMSO-normalised cell viability of DMSO- and 250 nM reversine-treated wild type or *cGas*^{KO} 4T1 cells supplemented with increasing quantities of IL6. **g)** Control DMSO-normalised cell viability of DMSO- or 500 nM AZD1775-treated wild type or *cGas*^{KO} 4T1 cells supplemented with increasing quantities of IL6. **h**–**j)** Control DMSO-normalised cell viability of DMSO- or 500 nM AZD1775-treated wild type, *cGAS*^{KO}, *STING*^{KO}, and *cGAS; STING*^{DKO} BT549 cells (**h**) wild type, *cGAS*^{KO}, *STAT3*^{KO}, or *cGAS*; *STAT3*^{DKO} BT549 cells (**i**), and wild type or *RelB*^{KO} BT549 cells (**j**) supplemented with increasing quantities of IL6. **k)** Control DMSO-normalised cell viability of DMSO- or 250 nM reversine-treated wild type or *cGAS*^{KO} BT549 cells supplemented with increasing quantities of IFNa2. **l)** Control DMSO-normalised cell viability of DMSO- or 500 nM AZD1775-treated wild type or *cGAS*^{KO} BT549 cells supplemented with increasing quantities of IFNa2. **m)** Control DMSO-normalised cell viability of DMSO- or 250 nM reversine-treated wild type, *cGAS*^{KO}, *STAT3*^{KO}, or *cGAS; STAT3*^{DKO} BT549 cells supplemented with increasing quantities of IFNa2. **n)** Control DMSO-normalised cell viability of DMSO- or 500 nM AZD1775-treated wild type, *cGAS*^{KO}, *STAT3*^{KO}, or *cGAS; STAT3*^{DKO} BT549 cells supplemented with increasing quantities of IFNa2. Grey lines in (**i**, **m**–**n**) represent replotted data from previous panels to simplify comparison. Error bars in all panels represent the s.e.m, n=3 biological replicates (**a**, **c**–**e**, **g**–**j**, **m**–**n**) n=4 biological replicates (**b**, **k**–**l**), n=5 biological replicates (**f**). Significance was tested with a two-sided t-test. *P<0.05, **P<0.01, ***P<0.005, exact P-values are specified in Source Data Extended Data Fig. 7. Cells were treated for 48 hours (**b**, **e**, **g**–**j**, **l**, **m**) or 72 hours (**c**, **d**, **f**, **k**, **m**).

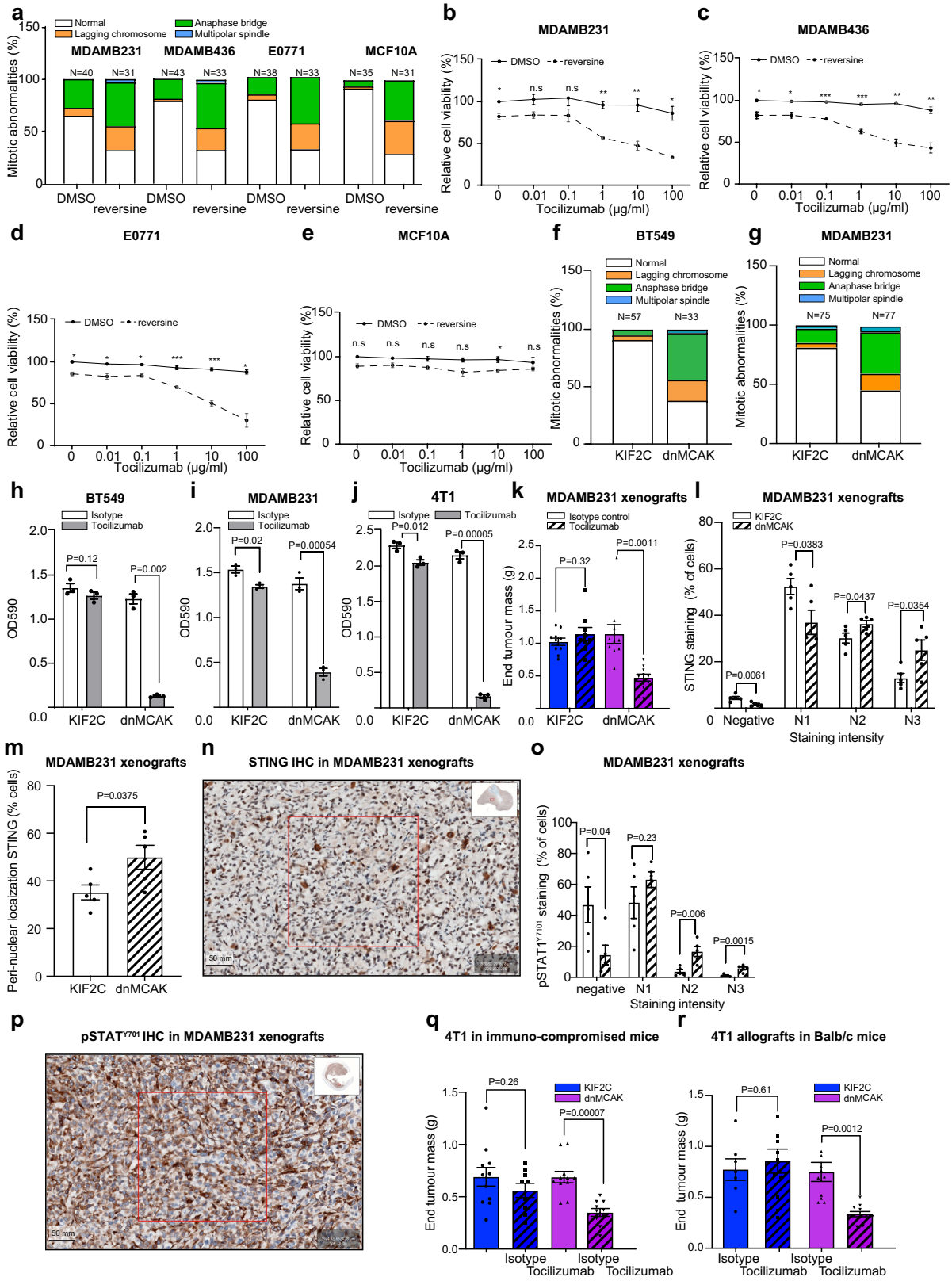

Extended Data Fig. 8 | See next page for caption.

Extended Data Fig. 8 | Tocilizumab treatment selectively targets TNBC cells but not untransformed mammary cells displaying CIN.
a) Quantification of mitotic abnormalities observed in MDAMB231, MDAMB436, E0771 or MCF10A cells expressing Histone H2B-cherry treated with DMSO or 250 nM reversine. **b**–**e)** Control DMSO-normalised cell viability of DMSO- or 250 nM reversine-treated MDAMB231(**b**), MDAMB436 (**c**), E0771 (**d**) and MCF10A (**e**) cells treated with increasing concentrations of tocilizumab. **f**–**g)** Quantification of mitotic abnormalities observed in Histone H2B-mCherry expressing KIF2C (CIN^{low}) or dnMCAK (CIN^{high}) BT549 cells (**f**) or MDAMB231 (**g**) assessed by live cell imaging, n indicates the number of assessed mitotic cells. **h**–**j)** Colony formation assay for isotype control- or 10 μM tocilizumab-treated BT549 (**h**), MDAMB231 (**i**), or 4T1 (**j**) cells expressing KIF2C (CIN^{low}) or dnMCAK (CIN^{high}). Cells were treated for a week. **k**) Weights of tumours extracted from immuno-compromised mice with xenografted MDAMB231 cells expressing KIF2C (CIN^{low}) or dnMCAK (CIN^{high}) treated with either tocilizumab or IgG control. Each dot represents a single tumour. **l**) Quantification of immunohistochemical staining for STING on KIF2C (CIN^{low})- or dnMCAK (CIN^{high})- expressing MDAMB231 xenografts. To quantify STING levels, cells were classified based on their staining intensity. Negative= no staining, N1= weak staining, N2= moderate staining, N=3 strong staining. **m)** Quantification of cells with perinuclear STING staining in MDAMB231 xenografts expressing KIF2C (CIN^{low})- or dnMCAK (CIN^{high}). **n)** Representative image for STING staining on an MDAMB231-xenografted tumour. Scale bar equals 50 μm. **o)** Quantification of immunohistochemical staining for phosphorylated STAT1 (p-$STAT^{Y701}$) on KIF2C (CIN^{low})- or dnMCAK(CIN^{high})-expressing MDAMB231 xenografts. To quantify p-$STAT1^{Y701}$ levels, cells were classified based on their staining intensity. Negative= no staining, N1= weak staining, N2= moderate staining, N=3 strong staining. **p)** Representative image for p-$STAT1^{Y701}$ staining on an MDAMB231-xenografted tumour. Scale bar equals 50 μm. **q**–**r)** Weights for tumours extracted from immunocompromised athymic (**q**) or immuno-proficient Balb/c (**r**) mice with xenografted 4T1 cells expressing KIF2C (CIN^{low}) or dnMCAK (CIN^{high}), treated with either tocilizumab or IgG. Each dot represents a single tumour. Error bars (**b**, **h**–**m**, **o**, **q**–**r**) represent the s.e.m., n=3 biological replicates (**b**–**e**, **h**–**j**), n=5 biological replicates (**l**–**m**, **o**), the number of replicates n is indicated in the panel (**k**, **q**, **r**), significance was tested using a two-sided t-test, * $P<0.05$, ** $P<0.01$, *** $P<0.005$, exact P-values are specified in Source Data Extended Data Fig. 8. Cells were treated for 96 hours (**b**–**e**).

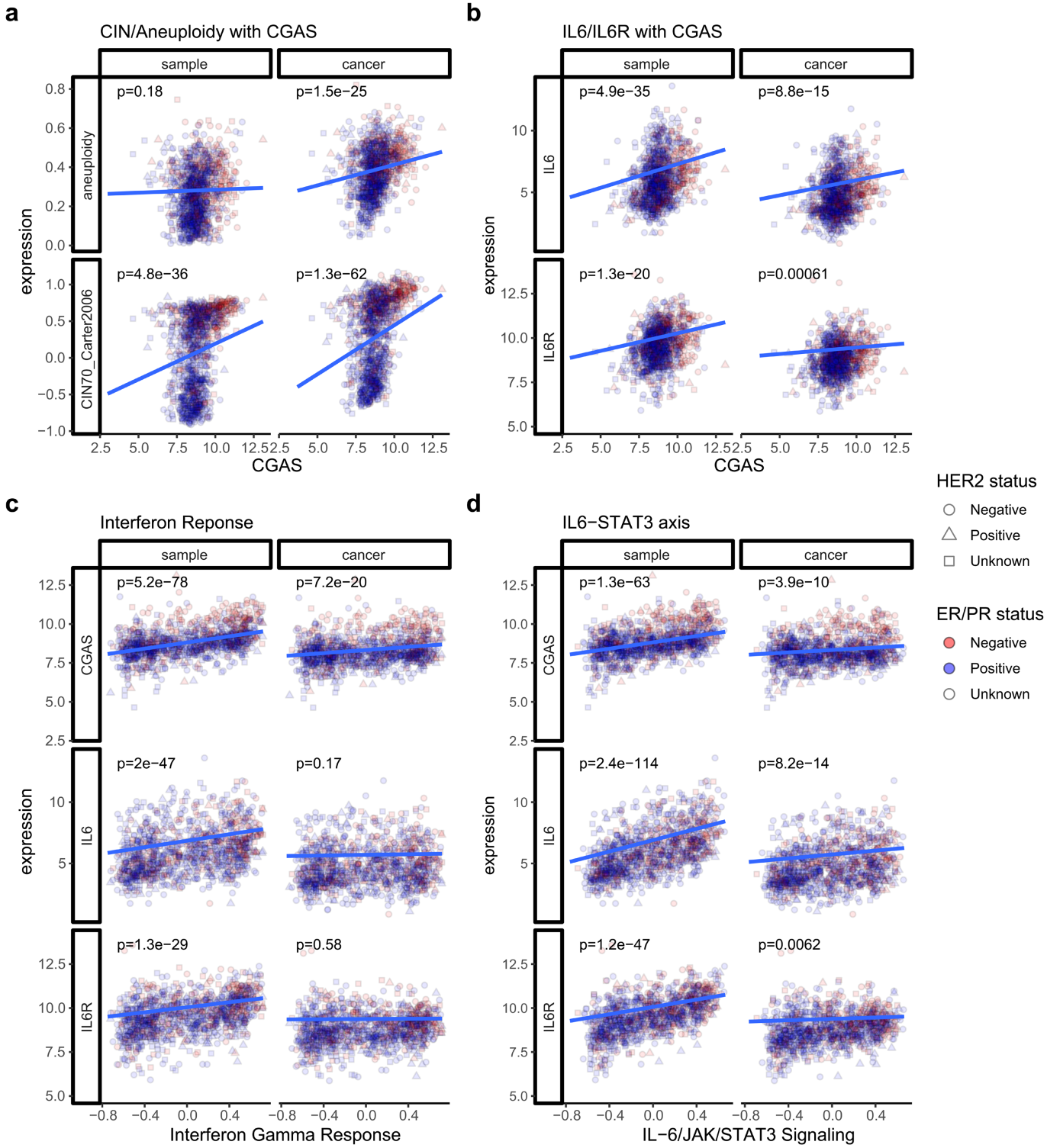

Extended Data Fig. 9 | See next page for caption.

Extended Data Fig. 9 | Correlations between CIN, aneuploidy, and IL6 and IL6R expression with cGAS expression or interferon activity in TCGA breast cancers. Expression levels of a gene (Variance Stabilizing Transformation) or gene set (Gene Set Variation Analysis, GSVA) are shown on both axes of each panel. Aneuploidy is measured by the average deviation of DNA copy number changes from the sample mean along the genome. Point colour indicates the hormone receptor status (red if both are negative, blue if either one or both are positive), and shape the HER2 amplification status by IHC. Panels labelled as "sample" show the value obtained from the tumour sample, "cancer" denotes the residual effect with the linear effect of sample impurity removed. **a)** cGAS expression correlates significantly with both aneuploidy and the CIN70 signature genes in the cancer cells, but not with aneuploidy when taking into account cancer and non-cancer cells (whole sample). This indicates that aneuploid cancer cells have a higher expression of cGAS than euploid cells, and this level is higher the more aneuploid the cancer cells are. **b)** cGAS expression correlates significantly with IL6 and IL6R expression irrespective of looking at the whole sample or the cancer-specific subset. The correlation is stronger in the whole sample, which indicates that IL6 expression is mainly driven by non-cancer cells in an aneuploidy-driven cancer environment, but the cancer cells themselves also increase their IL6 expression with increased aneuploidy. **c)** Interferon response genes correlate significantly with cGAS, IL6, and IL6R expression when taking into account the whole sample, but not with IL6 and IL6R expression for the cancer-only population. This indicates that cancer-specific IL6 and IL6R expression are independent of the cancer-intrinsic interferon response, potentially due to oncogenic adaptation to CIN[4]. **d)** IL6-STAT3 signalling correlates significantly with cGAS, IL6, or IL6R irrespective of looking at the sample or the cancer-specific population. This indicates that cancer cells themselves increase cGAS, IL6 and IL6R expression with increasing aneuploidy.

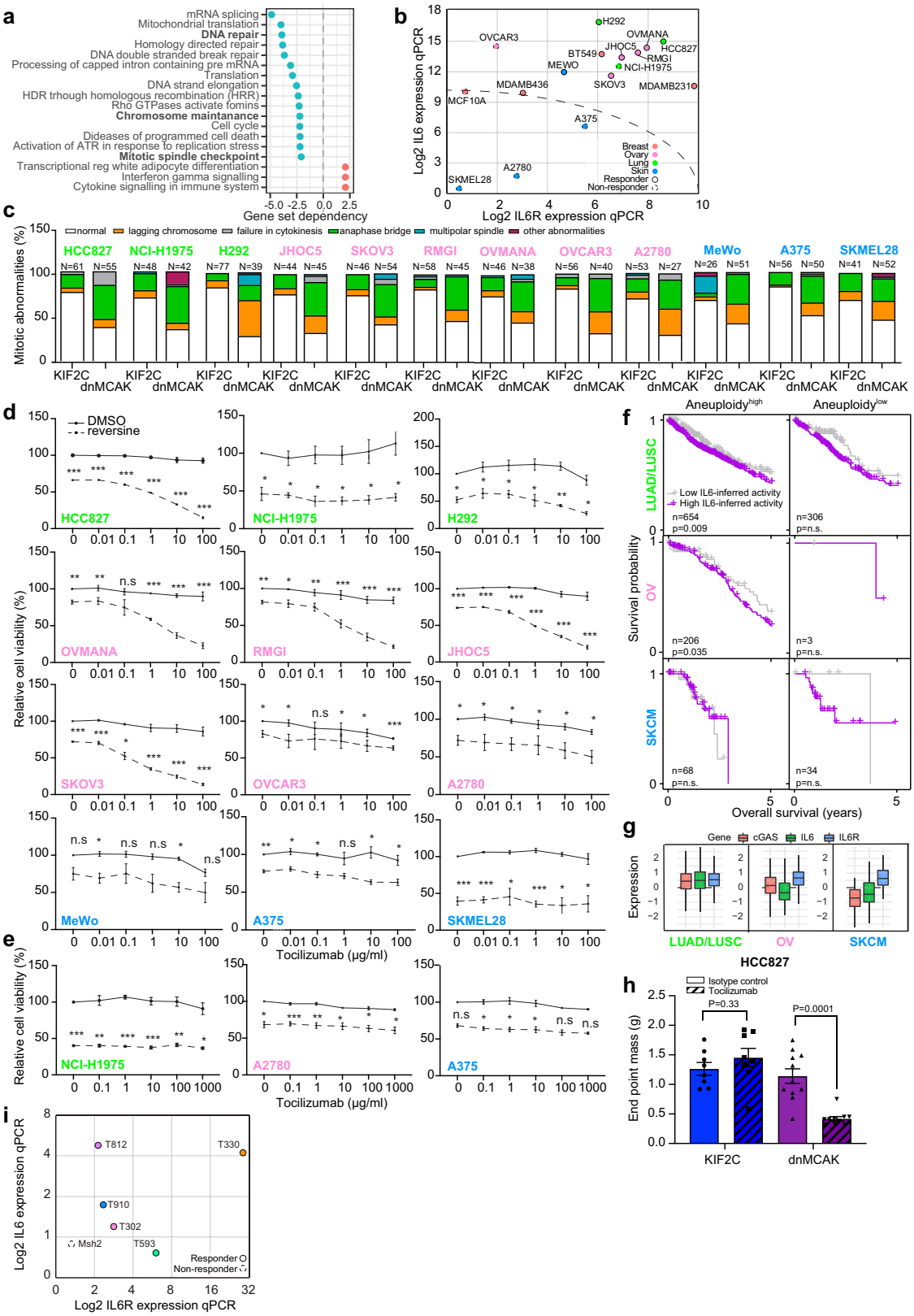

Extended Data Fig. 10 | See next page for caption.

Extended Data Fig. 10 | Tocilizumab selectively kills cancer cells with induced acute or chronic CIN across various cancer types dependent on IL6 and IL6R expression levels. a) REACTOME gene set enrichment for genes that become less essential with increasing IL6R mRNA levels in a DepMap analysis. Significance was tested using a student's t-test. **b)** Relative expression for IL6 and IL6R for all cell lines used in this study assessed by quantitative RT-qPCR. Expression of IL6 and IL6R were normalised to the lowest IL6 and IL6R expressing cell line, SKMEL28. Samples were measured in technical triplicate. Note that the results are in good agreement with the DepMap-annotated expression data, except that OVCAR3 and NCIH1975 cells express more IL6 in our experiment than reported in DepMap. **c)** Quantification of mitotic abnormalities in indicated cancer cell lines (lung cancers, skin cancers, and ovarian cancers) expressing KIF2C (CIN^{low}) or dnMCAK (CIN^{high}). **d)** Control DMSO-normalised cell viability of DMSO- or reversine-treated cells treated with increasing concentrations of tocilizumab. Top row: lung cancer cell lines, middle rows: ovarian cancer cell lines, and bottom row: skin cancer cell lines. JHOC5, A375, A2780, RMGI, OVCAR3, OVMANA, MEWO, and SKMEl28 were treated with 150 nM reversine. HCC827, H292, SKOV3, and NCI-H1975 with 250 nM reversine. **e)** Control DMSO-normalised cell viability of A2780 (ovarian cancer), NCI-H1975 (lung cancer), or A375 (skin cancer) treated with tocilizumab concentrations up to 1 mg/ml. **f)** Stratification of patient survival for aneuploid (left) and euploid (right) lung (LUAD, LUSC; top two panels), ovarian (OV, middle two panels) and skin cancers (melanoma; SKCM, bottom two panels) in the TCGA, matched for the functional cell line validation. Lung and ovarian tissues show a significant decrease in overall survival with active cancer-cell intrinsic IL6 signalling, melanoma does not. No tissue showed a survival effect with cGAS/IL6 for euploid cancers, but it should be noted that the sample number of euploid skin and ovarian cancers is low. **g)** Relative expression (z-score) of cGAS, IL6 and IL6R across the tissues used for validation in the TCGA. Lung cancers show high expression of all three, ovarian moderate expression of cGAS and IL6. Melanoma shows low expression of cGAS, potentially explaining the lack of cGAS/IL6-driven survival difference in (**f**). Boxes represent median +/− quartiles, whiskers indicate the 1.5 inter-quartile range. **h)** Weights for tumours extracted from immuno-compromised mice with xenografted HCC827 lung cancer cells expressing KIF2C (CIN^{low}) or dnMCAK (CIN^{high}) treated with either tocilizumab or IgG control. Each dot represents a single tumour. **i)** Relative expression for IL6 and IL6R for primary T-ALL cultures used in this study assessed by quantitative RT PCR. Expression of IL6 and IL6R were normalised to the lowest IL6 and IL6R expressing T-ALL culture, $Msh2^{-/-}$ (eT) cells. Samples were measured in technical triplicate. Error bars in (**d**–**e**, **h)** represent the s.e.m, n=3 biological replicates (**d**–**e**), number of replicates n is indicated in the figure (**g**), significance was tested by a two-sided t-test. * P<0.05, ** P<0.01, *** P<0.005, exact P-values are specified in Source Data Extended Data Fig. 10. Cells were treated for 96 hours (**d**–**e**).

nature portfolio

Corresponding author(s): Dr. Floris Foijer

Last updated by author(s): Apr 20, 2022

Reporting Summary

Nature Portfolio wishes to improve the reproducibility of the work that we publish. This form provides structure for consistency and transparency in reporting. For further information on Nature Portfolio policies, see our Editorial Policies and the Editorial Policy Checklist.

Statistics

For all statistical analyses, confirm that the following items are present in the figure legend, table legend, main text, or Methods section.

n/a	Confirmed	
☐	☒	The exact sample size (*n*) for each experimental group/condition, given as a discrete number and unit of measurement
☐	☒	A statement on whether measurements were taken from distinct samples or whether the same sample was measured repeatedly
☐	☒	The statistical test(s) used AND whether they are one- or two-sided *Only common tests should be described solely by name; describe more complex techniques in the Methods section.*
☒	☐	A description of all covariates tested
☒	☐	A description of any assumptions or corrections, such as tests of normality and adjustment for multiple comparisons
☒	☐	A full description of the statistical parameters including central tendency (e.g. means) or other basic estimates (e.g. regression coefficient) AND variation (e.g. standard deviation) or associated estimates of uncertainty (e.g. confidence intervals)
☐	☒	For null hypothesis testing, the test statistic (e.g. *F*, *t*, *r*) with confidence intervals, effect sizes, degrees of freedom and *P* value noted *Give P values as exact values whenever suitable.*
☒	☐	For Bayesian analysis, information on the choice of priors and Markov chain Monte Carlo settings
☒	☐	For hierarchical and complex designs, identification of the appropriate level for tests and full reporting of outcomes
☒	☐	Estimates of effect sizes (e.g. Cohen's *d*, Pearson's *r*), indicating how they were calculated

Our web collection on statistics for biologists contains articles on many of the points above.

Software and code

Policy information about availability of computer code

Data collection	ImageStudio, Deltavision Softworx version 6.0.0, BD FACSDivaSoftware version 6.1.3, ImageScope version 12.1
Data analysis	PRISM 9 Software from Graphpad, R studio version 3.6.3, ImageJ Software 1.48v, ICY Software, Flowjo Software V10, Snapgene version 6, ImageScope version 12.1, DESeq2 version 1.31.3, bcl2fastq version 1.8.4, HISAT2 version 2.1.0, Cutadapt version 1.12, FastQC version 0.11.8 Analysis code is available at https://github.com/mschubert/cgas_ko

For manuscripts utilizing custom algorithms or software that are central to the research but not yet described in published literature, software must be made available to editors and reviewers. We strongly encourage code deposition in a community repository (e.g. GitHub). See the Nature Portfolio guidelines for submitting code & software for further information.

Data

Policy information about availability of data

All manuscripts must include a data availability statement. This statement should provide the following information, where applicable:

- Accession codes, unique identifiers, or web links for publicly available datasets
- A description of any restrictions on data availability
- For clinical datasets or third party data, please ensure that the statement adheres to our policy

RNA sequencing data has been deposited at ArrayExpress under accession number E-MTAB-10923. Shallow single cell whole genome sequencing data has been deposited at ENA under accession number PRJEB49800.

Field-specific reporting

Please select the one below that is the best fit for your research. If you are not sure, read the appropriate sections before making your selection.

☒ Life sciences ☐ Behavioural & social sciences ☐ Ecological, evolutionary & environmental sciences

For a reference copy of the document with all sections, see nature.com/documents/nr-reporting-summary-flat.pdf

Life sciences study design

All studies must disclose on these points even when the disclosure is negative.

Sample size	Up to 6 mice per experimental group (4T1 allografted to Balb/c or athymic nude treated with Tocilizumab experiment), 4 mice per experimental group (4T1 WT, cGASKO, or STINGKO allograft experiment), 6 mice per experimental group (HCC827 and MDA MB 231 xenograft experiment). All in vivo data are expressed as mean ± s.e.m. Sample size was determined using power analysis with 90% power and 95% confidence. Based on the power calculation, we determined up to 6 mice per group was required for Tocilizumab experiment and up to 4 mice for the genetically modified 4T1 experiment.
Data exclusions	Tumors with volume below 80 mm3 at the time when treatment started were excluded from analysis.
Replication	All the in vitro experiments were repeated at least twice independently. For in vivo experiment, each tumor derived from mice is considered a replicate
Randomization	For in vivo experiment, when a tumor reached 100 mm3, treatment whether with isotype or tocilizumab was randomly assigned. For in vitro experiments, no randomization was carried out.
Blinding	Investigators were not blinded to the group allocation as the investigators were also responsible in recording tumor measurement and administering designated treatment.

Reporting for specific materials, systems and methods

We require information from authors about some types of materials, experimental systems and methods used in many studies. Here, indicate whether each material, system or method listed is relevant to your study. If you are not sure if a list item applies to your research, read the appropriate section before selecting a response.

Materials & experimental systems

n/a	Involved in the study
☐	☒ Antibodies
☐	☒ Eukaryotic cell lines
☒	☐ Palaeontology and archaeology
☐	☒ Animals and other organisms
☒	☐ Human research participants
☒	☐ Clinical data
☒	☐ Dual use research of concern

Methods

n/a	Involved in the study
☒	☐ ChIP-seq
☐	☒ Flow cytometry
☒	☐ MRI-based neuroimaging

Antibodies

Antibodies used

For immunoblotting:
cGAS;Cell Signaling;Clone D1D3G; 15102S, 1:1000
cGAS (mouse specific);Cell Signaling;Clone D3O8O; 31659S, 1:1000
STING;Cell Signaling;Clone D2PF2F; 13647S, 1:1000
IRF3;Cell Signaling;Clone D83B9; 4302S, 1:1000
STAT1;Cell Signaling;9172S, 1:1000
STAT3;Cell Signaling;Clone 124H6; 124H6S, 1:1000
NF-kB p65;Cell Signaling;Clone D14E12; 8242S, 1:1000
RelB;Cell Signaling;Clone D7D7W; 10544S, 1:1000
TRAF2;Cell Signaling;Clone C192; 4724S, 1:1000
NIK;Cell Signaling;4994S, 1:1000
β-actin;Cell Signaling;Clone 8H10D10; 3700S, 1:5000
Phospho-IRF3 Serine 396;Cell Signaling;Clone E7J8G; 37829S, 1:1000
Phospho-STAT1 Tyrosine 701;Cell Signaling;Clone 58D6; 9167S, 1:1000
Phospho- STAT3 Tyrosine 705;Cell Signaling;Clone D3A7; 9145S, 1:1000
IRDye 800CW Goat anti-Rabbit IgG (H + L);Licor;926-32211, 1:15000
IRDye 680RD Goat anti-Mouse IgG (H + L);Licor;926-68070, 1:20000
Anti-rabbit IgG, HRP-linked;Cell Signaling;7074S 1:2000

Anti-mouse IgG, HRP-linked;Cell Signaling;7076S 1:2000

For immunofluorescence:
cGAS;Cell Signaling;Clone D1D3G; 15102S, 1:250
STING;Cell Signaling;Clone D2PF2F; 13647S, 1:250
Rat-anti-BrdU (CldU);Abcam;Ab6326, 1:200
Mouse-anti-BrdU (IdU);BD Biosciences;Clone B4; BDB347580 1:200
Secondary Alexa555 goat-anti-rabbit;Invitrogen;A27039, 1:500
Secondary Alexa488 conjugated goat-anti-rat;Invitrogen;A-11006, 1:500
Secondary Alexa646 conjugated goat-anti-mouse;Invitrogen;A-21235, 1:500

For immunohistochemistry:
STING;Cell Signaling;Clone D2PF2F; 13647S, 1:100
Phospho-STAT1 Tyrosine 701;Cell Signaling;Clone 58D6; 9167S, 1:200
Goat-anti-rabbit-HRP;Agilent Dako;P044801-2
Rabbit-anti-goat-HRP; Agilent Dako;P0449

For flow cytometry:
FITC-conjugated Annexin V; Biolegend; 640905, 1:250

Validation

Antibodies were validated by the companies we purchased the antibodies from. The validation process adapted the work by Uhlen, et.al, ("A Proposal for Validation of Antibodies", Nature Methods (2016))

Eukaryotic cell lines

Policy information about cell lines

Cell line source(s)

4T1 (ATCC, CRL-2539), BT549 (ATCC, HTB-122), MDA-MB-231 (ATCC, CRM-TB-26), MDA-MB-436 (ATCC, HTB-130), E0771 (ATCC, CRL-3461), MCF10A (ATCC, CRL-10317), HCC827 (ATCC, CRL-2868), NCI-H1975 (ATCC, CRL-5908), H292 (ATCC, CRL-1848), OVMANA (JCRB Cell Bank, JCRB1045), RMGI (JCRB Cell Bank, JCRB0172), JHOC5 (RIKEN Cell Bank, RCB1520), SKOV3 (ATCC, HTB-77), OVCAR3 (ATCC, HTB-161), A2780 (Sigma Aldrich, 93112519), Mewo (ATCC, HTB-65), A375 (ATCC, CRL-1619), SKMEL28 (ATCC, HTB-72), Phoenix Ampho (ATCC, CRL-3213), 293T (ATCC, CRL-3216).

Authentication

Provided by vendor using the STR method

Mycoplasma contamination

None; mycoplasma tests were carried out regularly

Commonly misidentified lines
(See ICLAC register)

None of the cell lines used are listed in the ICLAC database

Animals and other organisms

Policy information about studies involving animals; ARRIVE guidelines recommended for reporting animal research

Laboratory animals

7 weeks old female Balb/c-OlaHsd, 7 weeks old female athymic Nude-Foxn1, and 7 weeks old female NOD:SCID (NOD.CgPrkdc<scid>Il2rg<tm1Wjl>/SzJ

Wild animals

This study did not involve wild animals

Field-collected samples

This study did not use field collected samples

Ethics oversight

All the procedures on the animal experiments were reviewed and approved by the Dutch Central Committee for animal testing (CCD) and local Animal Welfare Committee (IvD) at the Central Animal Facility of University Medical Centrum Groningen (UMCG). Mice were housed under specific pathogen-free conditions, maintained on a 12 hours light-dark cycle and given water and food ad libitum in the animal facility in accordance with animal care regulations.

Note that full information on the approval of the study protocol must also be provided in the manuscript.

Flow Cytometry

Plots

Confirm that:

☒ The axis labels state the marker and fluorochrome used (e.g. CD4-FITC).

☒ The axis scales are clearly visible. Include numbers along axes only for bottom left plot of group (a 'group' is an analysis of identical markers).

☒ All plots are contour plots with outliers or pseudocolor plots.

☒ A numerical value for number of cells or percentage (with statistics) is provided.

Methodology

Sample preparation	In order to quantify apoptosis, BT549 or 4T1 cells were treated as indicated and harvested. Cells were then stained with FITC-Conjugated Annexin V antibody (Biolegend, 640914) according to manufacturer's instruction. Upon completion of staining, cells were resuspended in FACS buffer (3% FBS in PBS) and analyzed using a Flow cytometry instrument.
Instrument	Data acquisition was performed with a BD FACS Canto II instrument
Software	Data acquisition was performed using BD FACSDiva Software and analysis was done with FlowJo V10
Cell population abundance	Not applicable because no sorting was performed
Gating strategy	First, we gated cell population on FSC-A vs SSC-A followed by singlets. We then identified the Annexin V positive and PI positive cells. Gates were set based on unstained control.

☒ Tick this box to confirm that a figure exemplifying the gating strategy is provided in the Supplementary Information.